Cell Reports
Medicine

Article

Targeting nucleic acid sensors in tumor cells to reprogram biogenesis and RNA cargo of extracellular vesicles for T cell-mediated cancer immunotherapy

Graphical abstract

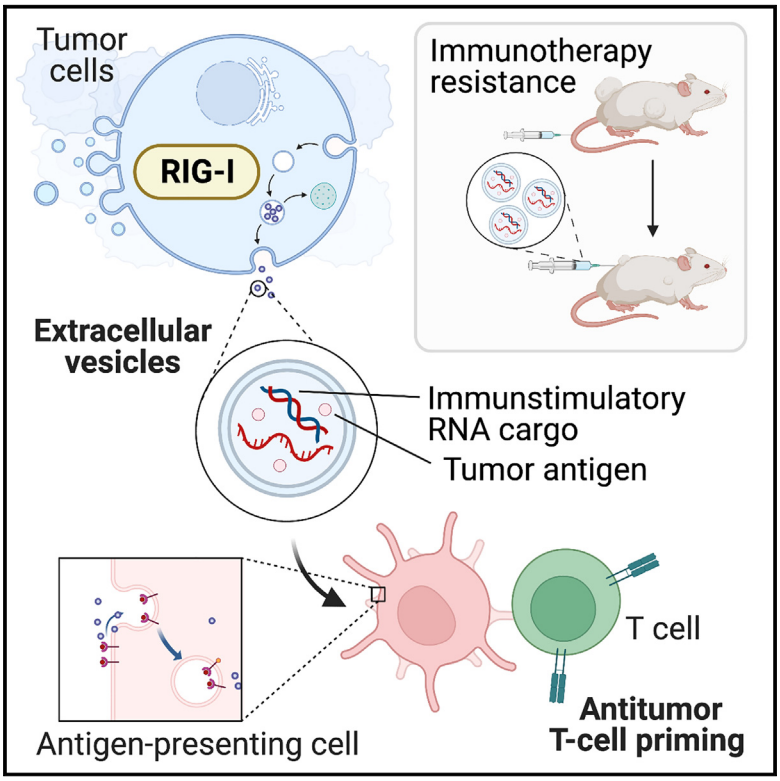

Highlights

- RIG-I activity regulates biogenesis and function of tumor cell-derived EVs
- Cancer-intrinsic RIG-I signaling governs the composition of the EV RNA cargo
- Immunostimulatory EVs trigger T cell-based antitumor immunity in mice and humans
- EV and RIG-I gene signatures in melanomas correlate with response to immunotherapy

Authors

Simon Heidegger, Florian Stritzke, Sarah Dahl, ..., Christoph Coch, Gunther Hartmann, Hendrik Poeck

Correspondence

simon.heidegger@tum.de (S.H.), hendrik.poeck@ukr.de (H.P.)

In brief

Extracellular vesicles harbor extraordinary potential for cancer therapy, but one limitation is an inadequate understanding of signaling pathways that regulate their biogenesis and function. Heidegger et al. define a tumor-intrinsic molecular pathway that can be targeted to modulate tumor EV cargo constituents and thus their immunomodulatory potential on T cell immunity.

Heidegger et al., 2023, Cell Reports Medicine *4*, 101171
September 19, 2023
https://doi.org/10.1016/j.xcrm.2023.101171

CellPress

Cell Reports Medicine

CellPress
OPEN ACCESS

Article

Targeting nucleic acid sensors in tumor cells to reprogram biogenesis and RNA cargo of extracellular vesicles for T cell-mediated cancer immunotherapy

Simon Heidegger,[1,2,20,21,*] Florian Stritzke,[1,2,3,20] Sarah Dahl,[1] Juliane Daßler-Plenker,[4,5] Laura Joachim,[1,2] Dominik Buschmann,[6] Kaiji Fan,[7] Carolin M. Sauer,[8] Nils Ludwig,[9] Christof Winter,[2,10,11] Stefan Enssle,[1,2] Suqi Li,[7] Markus Perl,[7] André Görgens,[12,13] Tobias Haas,[1] Erik Thiele Orberg,[1,2,10] Sascha Göttert,[7] Catherine Wölfel,[14] Thomas Engleitner,[2,15] Isidro Cortés-Ciriano,[8] Roland Rad,[2,10,15,16] Wolfgang Herr,[7] Bernd Giebel,[13] Jürgen Ruland,[2,10,11] Florian Bassermann,[1,2,10] Christoph Coch,[4,17] Gunther Hartmann,[4] and Hendrik Poeck[7,18,19,22,23,*]

[1]Department of Medicine III, School of Medicine, Technical University of Munich, Munich, Germany
[2]Center for Translational Cancer Research (TranslaTUM), School of Medicine, Technical University of Munich, Munich, Germany
[3]Department of Radiation Oncology, Heidelberg University Hospital, Heidelberg, Germany
[4]Institute of Clinical Chemistry and Clinical Pharmacology, University Hospital Bonn, Bonn, Germany
[5]Cold Spring Harbor Laboratory, Cold Spring Harbor, NY, USA
[6]Division of Animal Physiology and Immunology, TUM School of Life Sciences Weihenstephan, Technical University Munich, Freising, Germany
[7]Department of Internal Medicine III, University Hospital Regensburg, Regensburg, Germany
[8]European Molecular Biology Laboratory, European Bioinformatics Institute, Hinxton, Cambridge, UK
[9]Department of Oral and Maxillofacial Surgery, University Hospital Regensburg, Regensburg, Germany
[10]German Cancer Consortium (DKTK), Partner Site Munich and German Cancer Research Center (DKFZ), Heidelberg, Germany
[11]Institute of Clinical Chemistry and Pathobiochemistry, School of Medicine, Technical University of Munich, Munich, Germany
[12]Clinical Research Center, Department of Laboratory Medicine, Karolinska Institute, Stockholm, Sweden
[13]Institute for Transfusion Medicine, University Hospital Essen, University of Duisburg-Essen, Essen, Germany
[14]Internal Medicine III, University Cancer Center and Research Center for Immunotherapy, University Medical Center Johannes Gutenberg University and German Cancer Consortium (DKTK), Partner Site Frankfurt/Mainz, Mainz, Germany
[15]Institute of Molecular Oncology and Functional Genomics, School of Medicine, Technical University of Munich, Munich, Germany
[16]Department of Medicine II, School of Medicine, Technical University of Munich, Munich, Germany
[17]Department of Neurosurgery, University Hospital Leipzig, Leipzig, Germany
[18]Leibniz Institute for Immunotherapy (LIT), Regensburg, Germany
[19]Center for Immunomedicine in Transplantation and Oncology (CITO), Regensburg, Germany
[20]These authors contributed equally
[21]Twitter: @HeideggerS_MD
[22]Twitter: @HendrikPoeck
[23]Lead contact
*Correspondence: simon.heidegger@tum.de (S.H.), hendrik.poeck@ukr.de (H.P.)
https://doi.org/10.1016/j.xcrm.2023.101171

SUMMARY

Tumor-derived extracellular vesicles (EVs) have been associated with immune evasion and tumor progression. We show that the RNA-sensing receptor RIG-I within tumor cells governs biogenesis and immunomodulatory function of EVs. Cancer-intrinsic RIG-I activation releases EVs, which mediate dendritic cell maturation and T cell antitumor immunity, synergizing with immune checkpoint blockade. Intact RIG-I, autocrine interferon signaling, and the GTPase Rab27a in tumor cells are required for biogenesis of immunostimulatory EVs. Active intrinsic RIG-I signaling governs composition of the tumor EV RNA cargo including small non-coding stimulatory RNAs. High transcriptional activity of EV pathway genes and RIG-I in melanoma samples associate with prolonged patient survival and beneficial response to immunotherapy. EVs generated from human melanoma after RIG-I stimulation induce potent antigen-specific T cell responses. We thus define a molecular pathway that can be targeted in tumors to favorably alter EV immunomodulatory function. We propose "reprogramming" of tumor EVs as a personalized strategy for T cell-mediated cancer immunotherapy.

INTRODUCTION

Cancer immunotherapy by immune checkpoint blockade (ICB) has shown great clinical efficacy for solid and hematologic malignancies, yet response heterogeneity to ICB remains a clinical challenge. Therefore, it is important to better understand the mechanisms driving ICB-induced antitumor responses and therapy resistance. Engagement of type I interferon (IFN-I)-inducing

cytosolic nucleic acid sensing pathways—particularly the cGAS/STING and RIG-I/MAVS pathways—is critical in generating antigen-specific antitumor immune responses.[1–4] The DNA sensor cGAS and the downstream effector STING constitute a cytosolic pattern recognition receptor system that recognizes cytosolic DNA derivates from exogenous (microbial pathogens, dead cells) and endogenous (e.g., mitochondrial damage) sources to trigger innate immune gene transcription and IFN-I production.[5,6] The success of ICB with anti-CTLA-4 and anti-PD-1 are both dependent on cGAS/STING signaling in the tumor microenvironment (TME).[1,4,7,8] The cytosolic RNA receptor RIG-I (encoded by *DDX58*) detects double-stranded 5′-triphosphate RNA (3pRNA) from exogenous and endogenous sources (e.g., viruses, bacteria, non-coding RNAs [ncRNAs]).[6,9,10] Downstream signaling via the adapter molecule MAVS and transcription factors IRF3/IRF7 can induce potent IFN-I production. Therapeutic targeting of cGAS/STING and RIG-I in the TME has demonstrated strong antitumor effects mediated via IFN-I production by host immune cells and simultaneous induction of regulated cell death in malignant cells.[3,11] We recently demonstrated that immunotherapy with anti-CTLA-4 and its combination with anti-PD-1 or radiation therapy rely on tumor cell-intrinsic activation of RIG-I but not STING signaling.[12,13] However, the mechanisms of tumor-host communication following activation of these nucleic acid receptor pathways within tumor cells remain elusive.

As a new paradigm in intercellular communication, information exchange via extracellular vesicles (EVs) has become the focus of intense research.[14,15] EVs are a heterogeneous group of membrane-encapsuled vesicles that are released from virtually all cells, including cancer cells. Depending on the mechanism of EV biogenesis, distinct groups can be distinguished: microvesicles/ectosomes are formed by direct outward budding of the plasma membrane, while exosomes originate from the endosomal system.[14] EVs carry a vast bioactive cargo consisting of proteins, lipids, metabolites, and nucleic acids, which vary greatly by type and functional state of their cellular source.[16] Intrinsic properties of EVs in regulating complex intracellular pathways in target cells have sparked widespread interest in their potential utility in the therapeutic control of cancer. EVs released within the TME have been predominantly regarded as immunosuppressive and adversarial to immunotherapy,[17] yet the role of EVs in cancer is likely dynamic and specific to cancer type, genetics, and stage. EVs were also found to elicit potent immune reactions in a context-dependent manner. Tumor-derived EVs can induce activation of dendritic cells (DCs) via transfer of tumor-associated antigens (TAAs) and subsequent cross-priming of specific T cells.[18,19] However, conditions under which cancer cells release such immunostimulatory EVs, the involved signaling pathways, and their impact on T cell-based antitumor immunity and, thus, interaction with clinically established immunotherapies remain unclear. We here systematically dissect key molecules governing the biogenesis, cargo, and immunomodulatory function of tumor EVs. We show that cancer-intrinsic cytosolic RIG-I/IFN-I signaling can be harnessed for the generation of immunogenic tumor EVs that trigger potent antitumor T cell responses and synergize with ICB cancer immunotherapy.

RESULTS

RIG-I signaling does not influence quantitative EV release from tumor cells

To determine the role of tumor cell-intrinsic RIG-I signaling on EV content and release, murine B16 melanoma cells expressing the model antigen ovalbumin (B16.OVA) were transfected with a well-established RIG-I ligand (*in vitro* transcribed 5′-triphosphorylated RNA, 3pRNA). Twenty-four hours later, melanoma-cell-derived EVs were enriched from the culture supernatant (SN) using mainly a precipitation-based assay. EV preparations were termed by their cellular origin: RIG-I-EVs for EVs from SN of B16.OVA cells with active RIG-I receptor signaling (induced by 3pRNA), and control EVs (Ctrl-EVs) from SN of untreated cells under steady-state conditions. The enriched EV preparations were analyzed by electron microscopy and quantified by nanoparticle tracking analysis (NTA). Particles were found to be homogenously sized with a median diameter of 130–140 nm and showed a uniform distribution of number and concentration in different samples (Figures S1A–S1D). Presence of EV marker proteins that are generally associated with exosomes (Alix, Flotillin 1, HSP70, CD81, CD63), and strong under-representation of negative quality control markers (cytochrome *c*, calnexin) were confirmed by western blot (Figures S1E and S1F), following the MISEV2018 consensus guidelines by the International Society for Extracellular Vesicles.[20] Active tumor cell-intrinsic RIG-I signaling did not impact on size, protein load, or the number of released particles. By contrast, genetic loss of RIG-I activity did not impact on the abundance of EV protein markers (Figure S1G).

Tumor cell-intrinsic RIG-I signaling mediates the release of immunogenic EVs

To assess the immunomodulatory capacity of tumor EVs released during active RIG-I signaling, bone marrow-derived DCs were exposed to B16.OVA melanoma-derived tumor EV preparations. If not stated otherwise, the amount of EVs was normalized to the amount of tumor cells that generated these EVs and not the absolute particle numbers. Tumor cell-derived EVs released under steady-state conditions (Ctrl-EVs) did not result in detectable levels of IFN-I in DC cultures (Figure 1A). In contrast, EVs released by tumor cells undergoing RIG-I signaling induced maturation and strong IFN-I production in DCs (Figures 1A and S2A). EVs released by melanoma cells that were transfected with a sequence-identical non-triphosphate, synthetic RNA (synRNA) did not induce IFN-I production in DCs. By similar precipitation of medium supplemented with 3pRNA complexed in liposomes in the absence of tumor cells (mock-EVs), we excluded that 3pRNA-liposomes (used to activate RIG-I signaling in tumor cells) were co-purified within tumor EV preparations. Activation of the cGAS/STING pathway resulted in the release of poorly immunostimulatory cGAS-EVs from melanoma cells with low-level IFN-I-inducing capacity in DCs. The immunostimulatory potential of RIG-I-induced EV preparations in DCs showed clear dose dependency (Figure S2B). Cationic lipids such as lipofectamine have previously been applied to increase cellular uptake and, thus, bioactivity of EVs.[21] For *in vitro* experiments, we found that lipofectamine could increase the bioactivity of low-dose EVs, while IFN-I

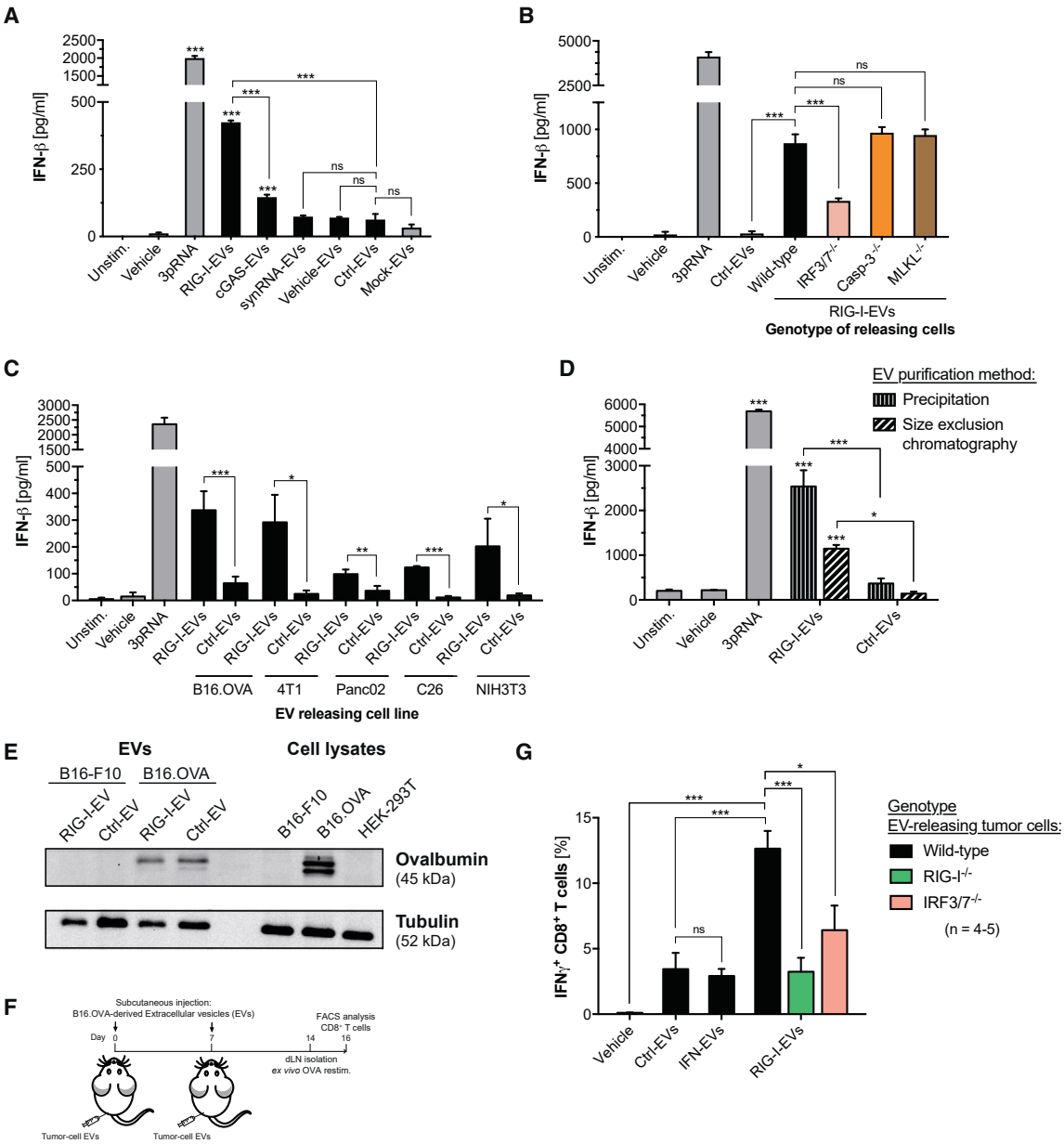

Figure 1. Tumor cell-intrinsic RIG-I signaling mediates the release of immunogenic EVs

B16.OVA melanoma cells were transfected with a RIG-I ligand (3p-RNA, RIG-I-EVs), interferon-stimulating DNA (cGAS-EVs), or synthetic RNA (synRNA-EVs). Extracellular vesicles (EVs) were enriched from the culture supernatant of treated and untreated (ctrl-EVs) cells. Precipitation of 3pRNA-liposomes in the absence of tumor cells was performed as negative control (mock-EVs).

(A) IFN-β release (ELISA) by dendritic cells (DCs) exposed to tumor cell-derived EV samples. Some DCs were directly transfected with *in vitro* transcribed 3pRNA as positive control.

(B–D) IFN-β release from DCs exposed to RIG-I-EV preparations: (B) prepared from different melanoma clones that lack specific downstream signaling components of nucleic acid receptor pathways; (C) enriched from various murine tumor cell lines: mammary (4T1), pancreatic (Panc02), colon (C26) carcinoma; and (D) enriched by precipitation or size-exclusion chromatography. All data are presented as mean values ± SEM of at least quadruplicate technical replicates per group and are representative of two independent experiments. Asterisks without brackets indicate statistical comparison with Ctrl-EV-treated cells.

(E) Presence of the antigen OVA (by western blot) in melanoma cell EV samples.

(F) Treatment model. C57BL6/j mice were repeatedly injected subcutaneously with tumor EV samples prepared from cultures of wild-type, RIG-I-deficient (RIG-I$^{-/-}$), or IRF3/7-deficient (IRF3/7$^{-/-}$) B16.OVA melanoma cells.

(G) IFN-γ release by CD8$^+$ T cells from draining lymph nodes after *ex vivo* OVA restimulation (flow cytometry).

Data are presented as mean values ± SEM of n = 4–5 individual mice per group and were pooled from two independent experiments. Unstim, unstimulated. See also Figures S1–S3.

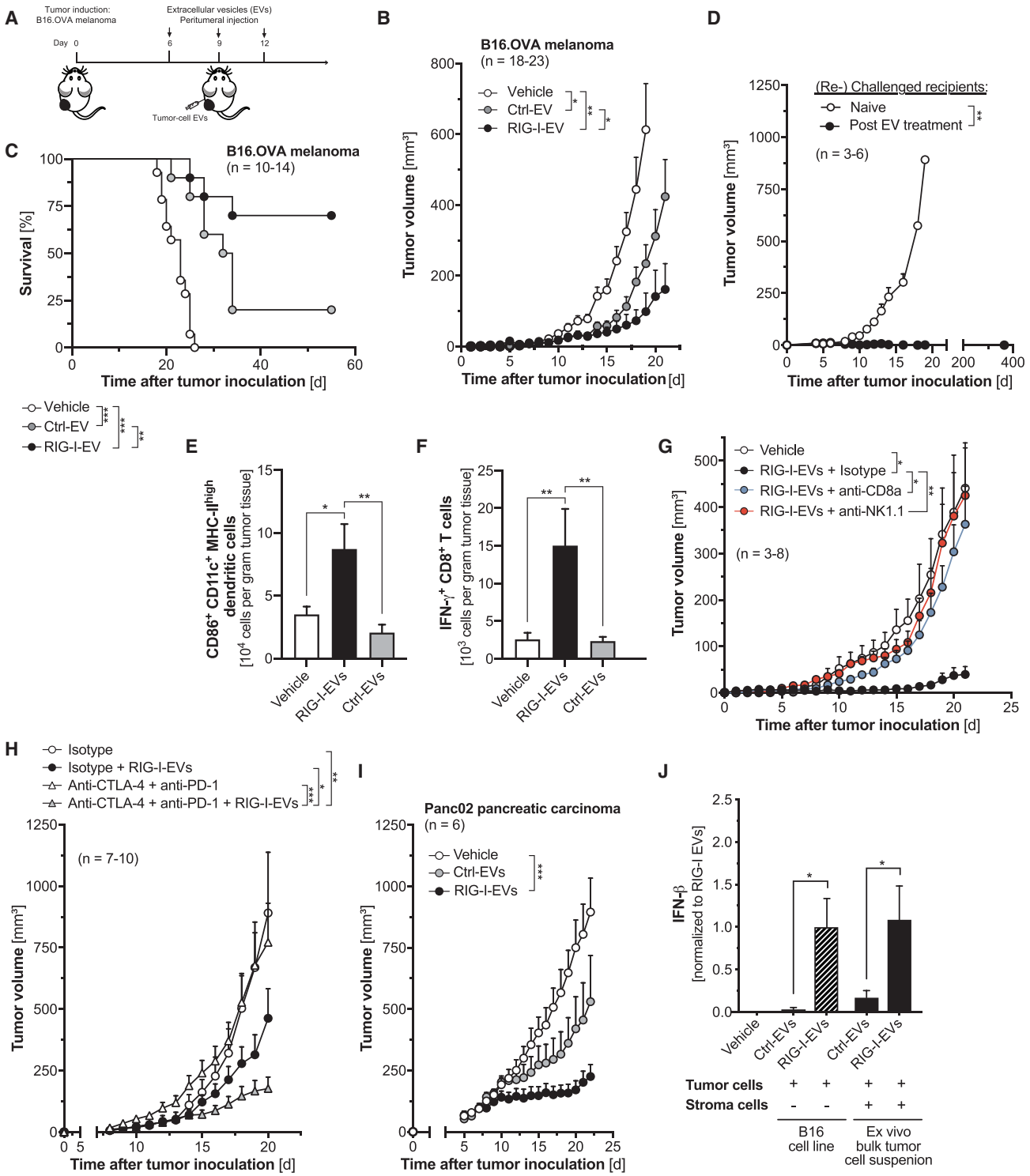

Figure 2. EVs released from RIG-I-activated tumor cells induce potent cytotoxic antitumor immunity and synergize with checkpoint inhibitors

(A) B16.OVA-bearing mice were injected peritumorally with melanoma-cell-derived EV samples.

(B and C) (B) Tumor growth and (C) overall survival.

(D) Tumor growth after rechallenge with a second, contralateral injection of viable B16.OVA cells in mice with initially complete tumor regression in response to EV treatment.

(E and F) Abundance of activated tumor-infiltrating (E) DCs and (F) $CD8^+$ T cells (n = 8–12 mice per group).

(legend continued on next page)

induction in DCs by exposure to high concentrations of EV preparations could not be further enhanced by application of lipofectamine (Figure S2B). If not stated otherwise, we used lipofectamine for *in vitro* experiments to increase the efficiency of low-dose EV treatment.

Next, we analyzed the molecular mechanisms downstream of RIG-I in the induction of immunostimulatory EV (isEV) release. The immunostimulatory capacity of tumor EVs released upon RIG-I activation was abrogated in tumor cells deficient for IRF3/7, two transcription factors central to the production of IFN-I (Figure 1B). We did not observe transfer of tumor cell-derived IFN-I in enriched tumor EV preparations (Figure S2C), yet activation of the RIG-I pathway within tumor cells can also induce an immunogenic form of programmed cell death[3,22,23] (Figure S2D). However, tumor-intrinsic genetic deficiency for the central executioner proteins of apoptosis (caspase-3) or necroptosis (MLKL), which prevents tumor cells from undergoing programmed cell death in response to RIG-I activation,[12] did not impact on the release of isEVs (Figure 1B). Furthermore, the immunostimulatory effect of RIG-I-induced EV preparations was observed in various murine tumor cell lines including mammary, pancreatic, and colorectal carcinomas, but also in non-transformed fibroblasts (Figure 1C). These data suggest that biogenesis and release of isEVs is a conserved cellular response pattern that requires coupling of cancer-intrinsic active RIG-I signaling to downstream IFN-I production via IRF3/7, but it occurs independent of regulated cell death.

Most methods used for EV enrichment co-isolate different EV populations of diverse biogenic origin.[14] Utilizing size-exclusion chromatography (SEC) or differential ultracentrifugation, we found that the immunostimulatory nature of RIG-I-induced EVs did not depend on the method used to enrich tumor EV preparations (Figures 1D and S2E–S2H). These very similar and overlapping findings for different enrichment assays imply that the RIG-I-induced immunostimulatory function is indeed mediated by isEVs and not by products of specific particle preparation methods.

Tumor-derived EVs have been attributed with the potential to induce efficient activation of DCs via transfer of TAAs and subsequent cross-priming of tumor-reactive T cells *in vivo*.[19] We found that B16.OVA melanoma-derived EVs indeed contained OVA antigen (Figure 1E). Shuttling of such TAA was not influenced by active RIG-I signaling in the EV-releasing cells. To better characterize the role of tumor cell-intrinsic RIG-I receptor pathway activity on the immunogenicity of tumor cell-released EVs *in vivo*, mice were immunized with B16.OVA-derived EV preparations, and T cell activation in draining lymph nodes was analyzed (Figure 1F). We found that immunization with isEVs released from melanoma cells during active RIG-I signaling showed strong immunogenic potential with potent activation of $CD8^+$ T cells *in vivo* (Figures 1G and S3A). Application of tumor EVs in mice was not associated with any clinically apparent signs of adverse events or systemic organ toxicity (Figure S3B). In line with our *in vitro* findings, the *in vivo* immunogenicity of RIG-I-induced isEVs was critically dependent on active RIG-I as well as IRF3/7 signaling in the EV-releasing tumor cells (Figure 1G). Without active simultaneous RIG-I signaling, *in vitro* treatment of tumor cells with recombinant IFN-I (IFN-EVs) was not sufficient to trigger the release of T cell-activating isEVs. Defective signaling of the RIG-I/IRF3/7 axis in tumor cells did not impact on quantitative EV release (Figure S3C). The potential of tumor cell-derived isEV preparations to induce T cell responses *in vivo* could be reproduced with complementary *ex vivo* EV enrichment methods such as SEC (Figure S3D). Tumor cell EVs also shuttled endogenous melanoma TAAs such as gp100 (Figures S3E and S3F). RIG-I-induced isEV preparations from otherwise poorly immunogenic B16-F10 melanoma were able to induce T cell immunity in the absence of artificial OVA antigen.

EVs released from RIG-I-activated tumor cells induce potent cytotoxic antitumor immunity and synergize with checkpoint inhibitors

Therapeutic application of isEVs enriched from *in vitro* RIG-I-activated B16.OVA cells showed strong antitumor effects accompanied by growth delay of melanomas *in vivo* with prolonged survival of tumor-bearing mice (Figures 2A–2C). Intriguingly, animals with stable tumor control after isEV treatment were protected against a second challenge with viable melanoma cells, indicating the formation of antitumor immunological memory (Figure 2D). Treatment with RIG-I-induced isEV preparations was associated with increased abundance of mature DCs as well as activated $CD4^+$ and $CD8^+$ T cells in the TME (Figures 2E, 2F, and S3G). The potent antitumor activity of isEVs was completely abrogated following antibody-mediated depletion of $CD8^+$ cytotoxic T cells (Figure 2G). Depletion of $NK1.1^+$ natural killer (NK) cells reduced the therapeutic efficacy of isEVs to a similar extent. In a melanoma model of suboptimal-dosed anti-PD-1/-CTLA-4, treatment with RIG-I-induced isEVs rendered tumors susceptible to ICB under conditions otherwise associated with tumor resistance to immunotherapy (Figure 2H). isEV preparations from syngeneic pancreatic tumor cells also showed high antitumor potency in a murine model of pancreatic carcinoma (Figure 2I). In possible translational use of tumor-derived isEVs as personalized tumor treatment, short-term culture of resected tumors may serve as a potential source of autologous isEV preparations. However, the composition of such *ex vivo* tumor cell cultures would be much more complex than the monoclonal murine tumor cell lines used here. At the same time, stromal-cell-derived EVs from cancer-associated fibroblasts have been postulated to harbor pro-tumorigenic function in the TME.[24] To account for the diversity of EVs within the TME, we generated EV preparations from short-term cultures of freshly isolated bulk tumor tissue. Similar to isEVs derived from homogeneous tumor cell lines, RIG-I stimulation resulted in the enrichment of isEV preparations from these heterogeneous cell cultures and subsequent induction of IFN-I in exposed DCs (Figure 2J).

(G and H) Tumor growth in mice additionally injected with (G) anti-CD8a- or anti-NK1.1-depleting antibodies, or (H) anti-PD-1/CTLA-4 checkpoint inhibitors.
(I) Panc02 pancreatic carcinoma growth in mice injected peritumorally with Panc02-cell-derived EV samples.
(J) IFN-β release from DCs exposed to RIG-I-induced EVs from either culture of B16.OVA melanoma cells or *ex vivo* cell suspensions of freshly isolated bulk tumors (mean ± SEM of n = 8 biological replicates pooled from at least three independent experiments).
All data are presented as mean tumor growth ± SEM and are pooled from or representative of at least two independent experiments. See also Figures S3 and S4.

As the basis for an alternative approach to harness the therapeutic potential of isEVs, we have previously shown that *in situ* vaccination with intra-tumoral injection of a RIG-I ligand has potent antitumor activity.[12,25] By analyzing a set of genes whose products were previously associated with vesicle secretion in tumor cell lines,[26] we found that targeted activation of RIG-I signaling in bulk tumors *in vivo* resulted in high transcriptional activity of vesiculation-associated genes (Figure 3A). The small guanosine triphosphatase Rab27a has been shown to be critically involved in the secretion of EVs of the endocytic biogenesis pathway.[27] Indeed, Rab27a deficiency in melanoma cells resulted in overall reduced numbers of released particles (Figures 3B–3D). In accordance with the dose dependency of isEV effects (Figure S2A), we found that reduced numbers of particles released by a fixed number of Rab27a$^{-/-}$ melanoma cells induced only low-level IFN-I production in DCs (Figure 3E). Mice bearing bilateral melanomas were *in situ* vaccinated by unilateral intratumoral injection of a RIG-I agonist (Figure 3F). The previously described[12] expansion of circulating tumor-antigen-specific T cells and systemic regression of tumors in response to RIG-I activation in the TME was largely diminished in mice bearing Rab27a$^{-/-}$ tumors (Figures 3G and 3H). These data suggest that (1) antitumor effects of *in situ* vaccination via tumor-intrinsic RIG-I activation rely in part on the production of EVs, and (2) the release of RIG-I-induced isEVs (but also Ctrl-EVs) depends on Rab27a-mediated EV biogenesis pathways.

Tumor cell-derived EVs are actively taken up by dendritic cells via endocytic pathways

Different mechanisms of EV uptake in recipient cells can have direct consequences for the distinct intracellular localization, degradation, and functional outcomes of EV constituents.[28] Tumor EV particles labeled with a fluorescent membrane marker showed rapid uptake by DCs, with an intracellular distribution pattern of the dye that suggested cytosolic delivery (Figures S4A and S4B). Blocking clathrin- and caveolin-dependent endocytosis (dynasore) or macropinocytosis (amiloride) with chemical inhibitors abrogated internalization of labeled particles by DCs (Figures S4C and S4D). Only inhibition of particle uptake via macropinocytosis prevented subsequent IFN-I induction in recipient DCs (Figure S4E). These data suggest that (1) tumor-derived EVs are actively ingested by DCs via endocytic pathways, and (2) the immunostimulatory effect of RIG-I-induced isEV preparations requires uptake via macropinocytosis in recipient cells. In fact, macropinocytosis of EVs has been associated with cytosolic delivery of cargo nucleic acids,[29] where they could in principle be detected by RIG-I/MAVS and/or cGAS/STING.

Immunogenicity of RIG-I-induced tumor isEVs is mediated via host nucleic acid receptor signaling and IFN-I activity in myeloid cells

Next, we aimed to identify the molecular pathways within host cells that are targeted by RIG-I-induced isEVs and their constituents. The importance of IFN-I signaling within host antigen-presenting cells (APCs) for the induction of antitumor T cell immunity has been widely acknowledged.[30,31] Using antibodies to block the common interferon-α receptor subunit 1 (IFNaR1), we found that T cell activation *in vivo* in response to RIG-I-induced EV preparations was critically dependent on host IFN-I signaling (Figure 4A). Furthermore, we applied isEV preparations in mice with conditional genetic deficiency that specifically lack IFNaR1 in either CD11c^{+} DCs or LysM^{+} macrophages. Hereby, we found that T cell activation by RIG-I-induced tumor isEVs depends on IFN-I receptor activity in both APC types (Figure 4B).

Activation of nucleic acid receptor signaling within host immune cells is a very potent stimulus for IFN-I release and has been found to be critical in the induction of antitumor immunity.[4] We treated mice that genetically lacked either the RIG-I adapter MAVS (*Mavs*$^{-/-}$) or the cGAS adapter STING (*Sting*$^{gt/gt}$) with tumor EVs, and found that isEV-induced T cell activation was largely abrogated in the absence of functional MAVS signaling within host cells (Figure 4C). Host cell deficiency for STING partially reduced T cell immunity in response to RIG-I-induced isEVs *in vivo*. To further characterize the role of host nucleic acid receptors in the detection of isEVs and their cargo, DCs derived from *Mavs*$^{-/-}$ or *Sting*$^{gt/gt}$ donor mice were exposed to melanoma-cell-derived EV samples *in vitro*. *Mavs*$^{-/-}$ DCs showed drastically reduced IFN-I production in response to RIG-I-induced isEVs (Figure 4D), while STING-deficient DCs only showed a partial defect in isEV detection *in vitro*. In contrast, genetic deficiency for Toll-like receptor 3 (TLR-3) or MyD88 (the adapter protein for the nucleic acid sensing TLRs 7–9) did not impact on the ability of DCs to release IFN-I upon interaction with RIG-I-induced isEVs (Figure 4E). These data suggest that RIG-I activity within tumor cells fosters the release of particularly immunogenic EVs that initiate IFN-I signaling within host APCs. This presumably happens via the transfer of RIG-I/MAVS-activating (and to a lesser extent cGAS/STING-activating) ligands, and subsequent activation of T cells.

Tumor-intrinsic RIG-I pathway activity mediates shuttling of immunostimulatory RNA within EVs

To address the possible transfer of immunostimulatory tumor RNA via EVs, we fluorescently labeled the bulk RNA cargo of tumor EV samples prior to their exposure to DCs. We observed concentration-dependent transfer of labeled EV RNA cargo to DCs (Figure 5A). Next, we extracted nucleic acids from tumor cell-derived EV samples and transfected DCs with liposome-bound EV RNA *in vitro*. We found that only RNA purified from RIG-I-induced isEV preparations induced potent IFN-I production in DCs (Figure 5B). Treatment of isEV-derived RNA with alkaline phosphatase to cleave 5′-triphosphate groups and, thus, the RIG-I-activating moiety significantly reduced its immunostimulatory capacity. However, despite alkaline phosphatase treatment, EV-extracted RNA still showed significant IFN-I induction in DCs, suggesting that immunostimulatory isEV-RNA is heterogeneous and is composed of both RIG-I-activating 3pRNAs and other non-RIG-I-targeting stimulatory RNAs. Exposure of tumor EV preparations to RNAse A, an endoribonuclease digesting single- and double-stranded RNA, did not impact on IFN-I production of recipient DCs (Figure S5A), suggesting that RNA in these samples was indeed shuttled inside membranous particles, protecting it from enzymatic degradation. Next, tumor cells were transfected with fluorescently labeled 3pRNA, and subsequently released isEVs were analyzed by imaging flow cytometry. We detected labeled, *in vitro* transcribed 3pRNA only within a very small fraction of tumor

CellPress
OPEN ACCESS

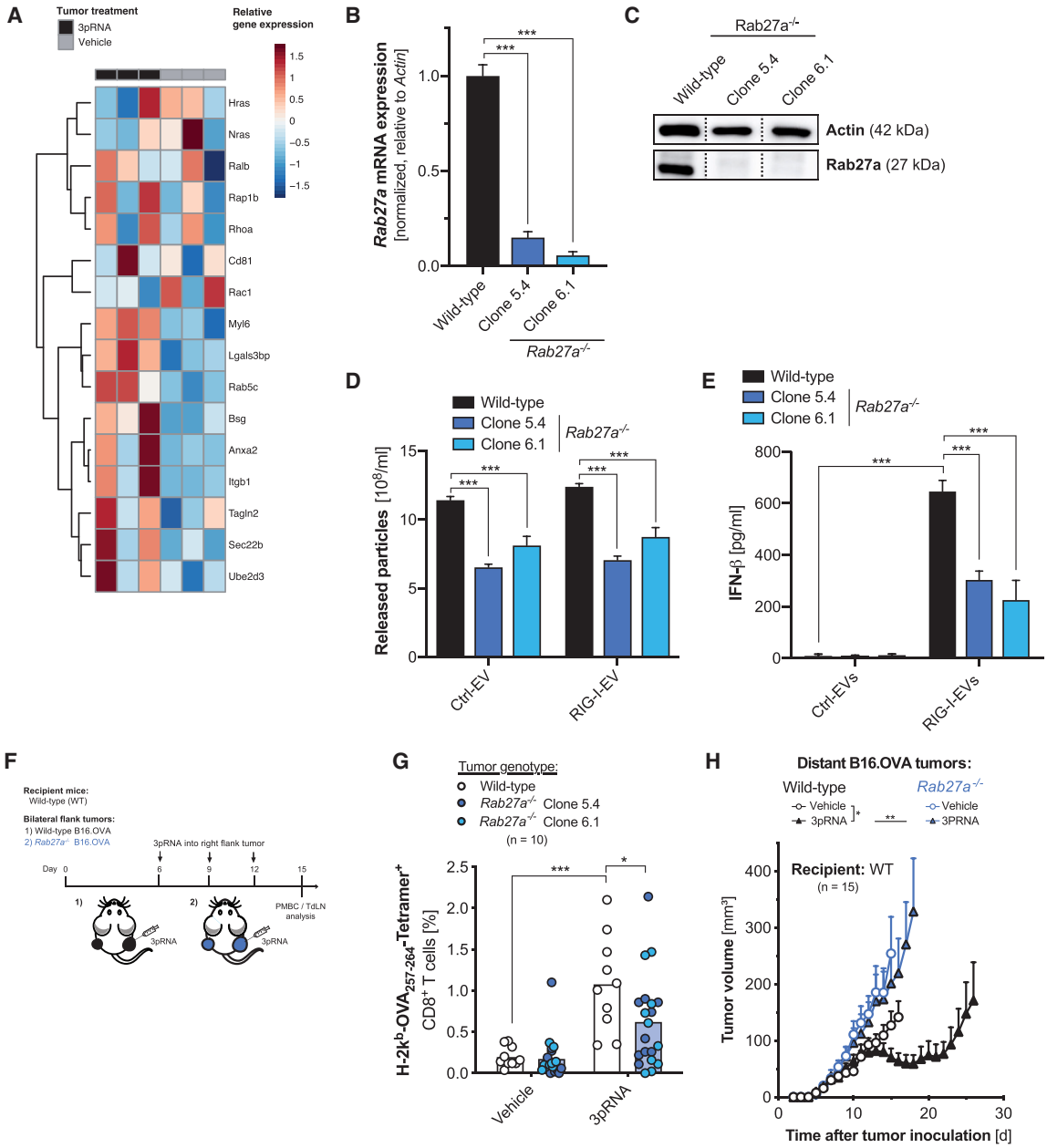

Figure 3. Therapeutic *in situ* activation of the RIG-I pathway modulates tumor EV generation for systemic antitumor immunity

(A) RNA-seq of bulk tumor after a single intratumoral injection of 3pRNA in B16.OVA melanoma-bearing mice. Heatmap shows *Z*-transformed expression of genes associated with tumor EV biogenesis and cargo loading.

(B and C) (B) Rab27a mRNA copy numbers of two different Rab27a-deficient (Rab27a$^{-/-}$) clones and (C) corresponding protein expression (western blot).

(D and E) EVs were enriched from Rab27a$^{-/-}$ B16 cell cultures. (D) Particle quantification within EV preparations by NTA. (E) IFN-I induction in DCs exposed to EVs from Rab27a$^{-/-}$ B16.OVA cells.

(F) Mice bilaterally bearing either wild-type or Rab27a$^{-/-}$ melanomas were injected with 3pRNA into right-sided tumors.

(G) Mean and individual frequency of H-2Kb-SIINFEKL tetramer^{+} CD8^{+} T cells in peripheral blood of n = 10 mice per group pooled from two independent experiments.

(H) Mean volume of left-sided tumors ± SEM of n = 15 individual mice per group pooled from three independent experiments.

All *in vitro* data show mean ± SEM of at least quadruplicate technical replicates, representative of at least two independent experiments.

cell-derived EVs (Figures S5B and S5C). After EV lysis with a detergent the fluorescence signal was no longer detectable, indicating that the RNA-bound fluorescent dye indeed accumulated within membranous EVs rather than unspecific protein aggregates (Figure S5D). Together with our findings that the generation of immunostimulatory EVs is dependent on active RIG-I signaling

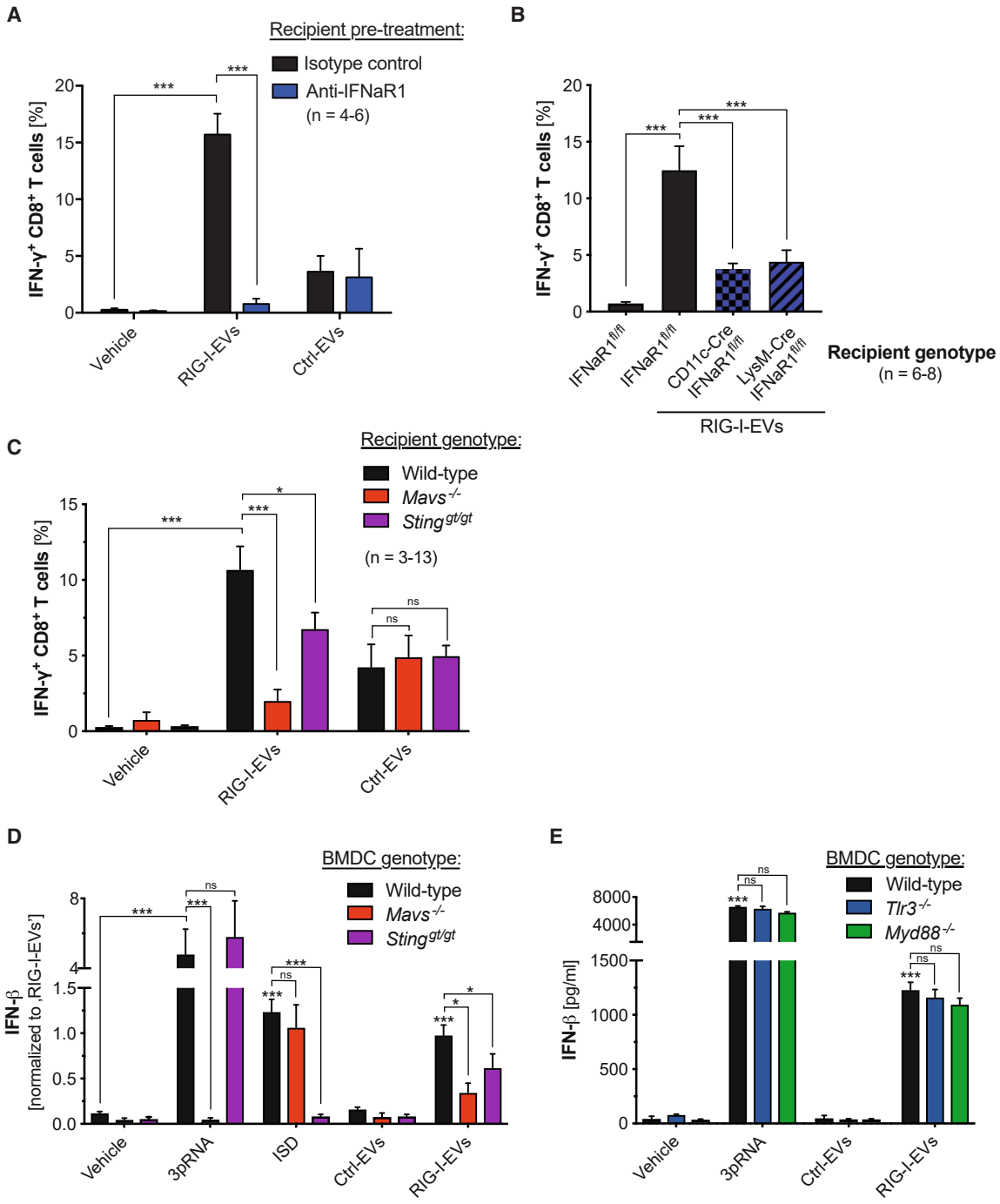

Figure 4. Immunogenicity of RIG-I-induced isEVs is mediated via host cytosolic nucleic acid receptor signaling and IFN-I activity in myeloid antigen-presenting cells

(A) Mice were treated with anti-IFNaR1 antibodies prior to immunization with B16.OVA melanoma cell EV samples. IFN-γ release by $CD8^+$ T cells (flow cytometry). (B and C) IFN-γ release by $CD8^+$ T cells upon tumor EV immunization in mice with genetic deficiency (B) for IFNaR1 in DCs (*CD11c-Cre Ifnar*$^{fl/fl}$) or macrophages (*LysM-Cre Ifnar*$^{fl/fl}$), and (C) globally for MAVS (*Mavs*$^{-/-}$) or STING (*Sting*$^{gt/gt}$). Data represent the mean value ± SEM of individual mice per group pooled from at least two independent experiments.

(D and E) IFN-I production in (D) *Mavs*$^{-/-}$ or *Sting*$^{gt/gt}$ DCs and (E) TLR-3-deficient (*Tlr3*$^{-/-}$) or Myd88-deficient (*Myd88*$^{-/-}$) DCs exposed *in vitro* to melanoma EV samples.

All *in vitro* data show mean ± SEM of at least triplicate technical replicates, representative of at least two independent experiments. Asterisks without brackets indicate statistical comparison to vehicle-treated control cells. See also Figure S4.

CellPress
OPEN ACCESS

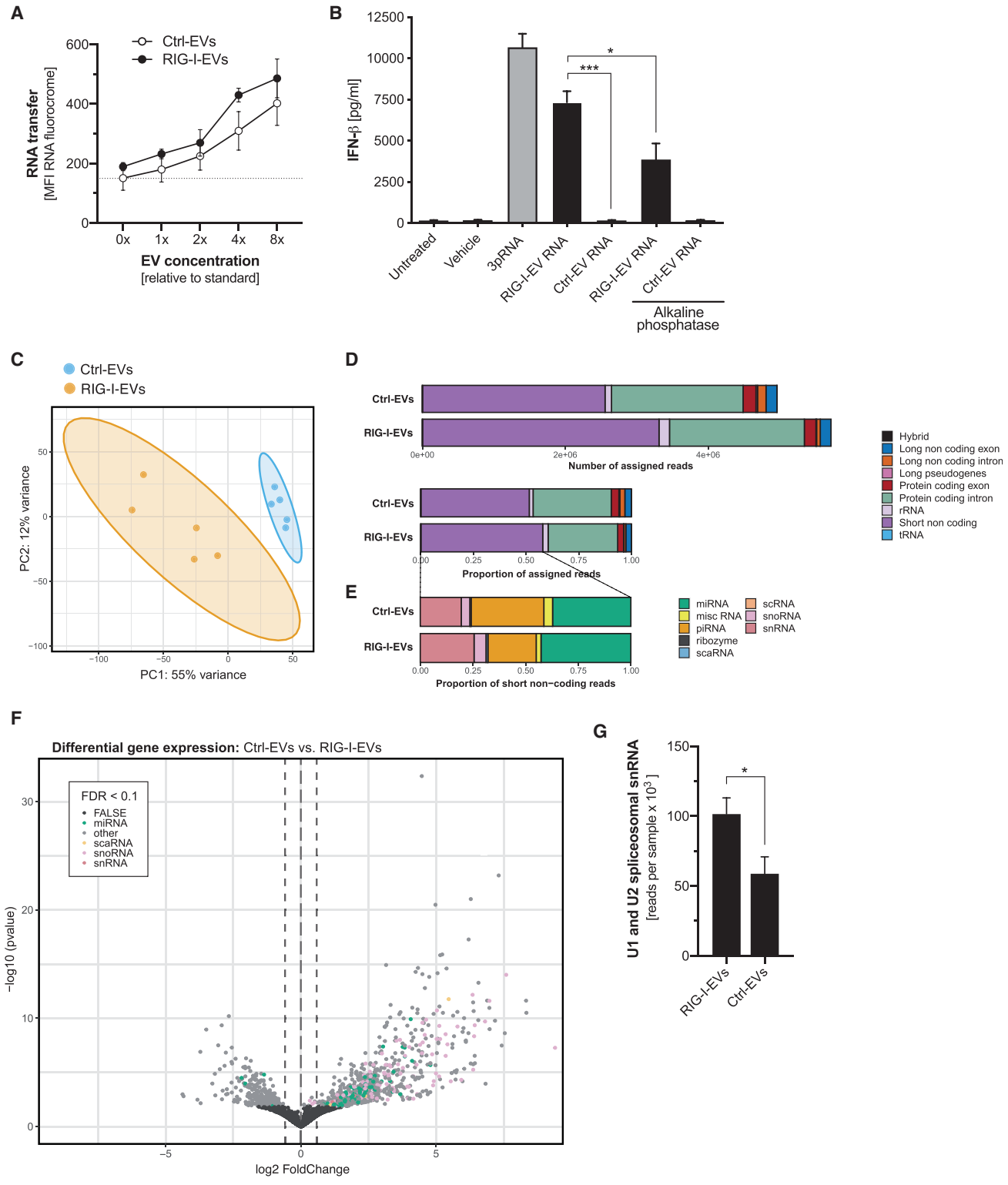

Figure 5. Tumor-intrinsic RIG-I pathway activity mediates shuttling of immunostimulatory RNA within EVs

(A) Transfer of EV RNA to DCs after exposure to B16 melanoma EVs with fluorescently labeled RNA cargo (flow cytometry).

(B) IFN-β release by DCs upon transfection with tumor EV extracted RNA or *in vitro* transcribed 3pRNA. Some EV RNA was treated with alkaline phosphatase prior to DC transfection (ELISA, mean value ± SEM of at least triplicate technical replicates, representative of at least two independent experiments).

(legend continued on next page)

in EV-releasing tumor cells (Figure 1G), these data speak against passive transfer of *in vitro* transcribed 3pRNA used for melanoma RIG-I activation into tumor isEVs in biologically relevant abundance.

The amount of DNA that we were able to extract from tumor cell EV preparations was drastically lower than for RNA (Figure S5E). We pooled the extracted DNA from very large numbers of tumor EV samples and transfected DCs with liposome-bound EV DNA. EV DNA induced IFN-I production in DCs via activation of the STING pathway (Figure S5F). However, its immunostimulatory potential was independent of active RIG-I signaling in EV-releasing tumor cells. Reduced IFN-I induction by EV preparations that were treated with DNase I prior to EV lysis for DNA extraction suggested that some EV DNA was surface-bound and not internal EV cargo. From this we concluded that RIG-I signaling in tumor cells results in the shuttling of different endogenous immunostimulatory RNAs within EVs. The biological role of tumor EV DNA is less clear. If anything, not qualitative but quantitative changes in EV DNA cargo might alter EV immunostimulatory function; but these changes seem independent of tumor cell-intrinsic RIG-I activity.

Cargo RNAs of EV include various biotypes that represent a selected portion of the RNA content of the source cell, with a strong bias toward small ncRNAs.[32] We performed next-generation sequencing of the endogenous RNA cargo extracted from tumor EV preparations. Given the proposed role of small nuclear RNA (snRNA) and small nucleolar RNA (snoRNA) as endogenous RIG-I ligands and their accumulation in the cytosol in tumor cells during cellular stress situations,[33] we performed library preparation and RNA sequencing (RNA-seq) optimized for the analysis of small RNAs. Hereby, we found that RIG-I signaling in tumor cells indeed actively shaped the global EV RNA composition (Figure 5C). Short ncRNAs were abundant in all tumor EVs (Figure 5D). However, active RIG-I signaling within the EV-releasing melanoma cells altered subsequent EV cargo composition with a general enrichment of snRNAs (Figures 5E and S6A) and a shift in the abundance of particular ncRNAs including snoRNAs (Figure 5F and Table S1). Some of the snRNA transcripts that were found to be particularly enriched in RIG-I-induced isEV preparations, such as the U1 and U2 spliceosomal RNAs (Figure 5G), have been implicated as endogenous ligands for cytosolic RIG-I-like helicases in tumor cells.[33] The RIG-I-activating endogenous ncRNA RN7SL1, which was previously described to promote tumor growth, metastasis, and therapy resistance in breast cancer cells after EV-mediated transfer,[24] was significantly less abundant in RIG-I-EVs (Figure S6B).

EVs can shuttle functional microRNA (miRNA) to regulate gene activity in distant target cells. However, to the best of our knowledge, none of the top hits among the 60 miRNAs we found to be differentially regulated in the EV cargo of RIG-I-activated tumor cells (Figure 5F and Table S2) have previously been linked to RIG-I-like receptor activity and/or EV function in the context of cancer. Additionally, ncRNAs arising from repetitive elements that are typically silenced yet often highly expressed in cancers have been implicated in the activation of innate immunity.[34] These ncRNAs were not found to be enriched in RIG-I-EVs (Figure S6C). Finally, even though our analysis was not designed to analyze long RNA, we identified mRNA fragments within the tumor EV cargo, the vast majority of which mapped to intronic regions (Figure 5D). For the mRNA exonic sequences, our data cannot evaluate whether they contain any full-length protein-encoding sequences or only mRNA fragments. Nevertheless, we performed gene set enrichment analysis (GSEA) and found that significantly enriched RNAs in the RIG-I-EV cargo mainly clustered in immune-related pathways (Figure S6D). Hereby, we found large overlap with the cellular transcriptome of RIG-I-activated melanoma cells, derived from a previously published GSEA of *ex vivo* bulk tumor RNA-seq.[12] These data confirm that the tumor EV RNA cargo reflects the cellular RNA content and show that RIG-I signaling activity in tumor cells results in the preferred shuttling of specific RNAs of different biotypes within tumor cell-derived EVs, thereby contributing to their immunostimulatory potential.

RIG-I signaling dictates the immunogenicity of EVs released by human melanoma cells

To assess translational relevance of our findings, we enriched EVs from culture supernatants of the human melanoma cell line D04mel under steady-state conditions (Ctrl-EVs) or active RIG-I signaling induced by 3pRNA (RIG-I-EVs). Peripheral blood mononuclear cells (PBMCs) from healthy donors were exposed to tumor EV preparations in *ex vivo* cultures. Uptake of carboxyfluorescein succinimidyl ester-labeled particles was largely restricted to monocytes but could also be observed in NK cells (Figure S7A). RIG-I-induced human tumor isEV samples stimulated potent release of IFN-I and the IFN-I-induced chemokine CXCL10 by the monocyte subpopulation within PBMCs (Figure 6A) but not of pro-inflammatory cytokines (Figures S7B and S7C). RNA extracted from tumor isEV preparations enriched from different RIG-I-activated human melanoma or non-malignant human primary fibroblast cultures showed immunostimulatory potential in PBMCs, which was largely abrogated when EV-extracted RNA was pretreated with 3pRNA-inactivating alkaline phosphatase (Figures 6B and S7D). Human DCs also potently produced IFN-I after exposure to RIG-I-induced melanoma isEV samples (Figure S7E). The immunostimulatory potential of EVs released from 3pRNA-treated human tumor cells was critically dependent on active RIG-I and autocrine IFN-I signaling but not cGAS/STING signaling (Figure 6C). Hereby, the level of tumor cell-intrinsic RIG-I expression correlated with the immunostimulatory capacity of released isEVs (Figure S7F). Tumor-derived EVs released during active cGAS or STING signaling in human tumor cells did not induce IFN-I in monocytic THP-1 cells

(C–G) RNA-seq of small RNA content extracted from B16.OVA melanoma cell EVs (n = 3 biological replicates per group). (C) Principal component analysis of the RNA content of Ctrl-EVs vs. RIG-I-EVs. (D) Absolute (upper panel) and relative abundance (lower panel) of the indicated RNA biotypes. (E) Relative abundance of the indicated short non-coding RNA. (F) Differential gene expression volcano plot of RNA content in RIG-I- vs. Ctrl-EVs. Significantly differentially expressed small non-coding RNAs are color-coded by their respective biotypes. (G) Cumulative abundance of U1 and U2 splicesosomal RNA reads in the RNA content of EVs, normalized to the overall library size.
See also Figures S5 and S6; Tables S1 and S2.

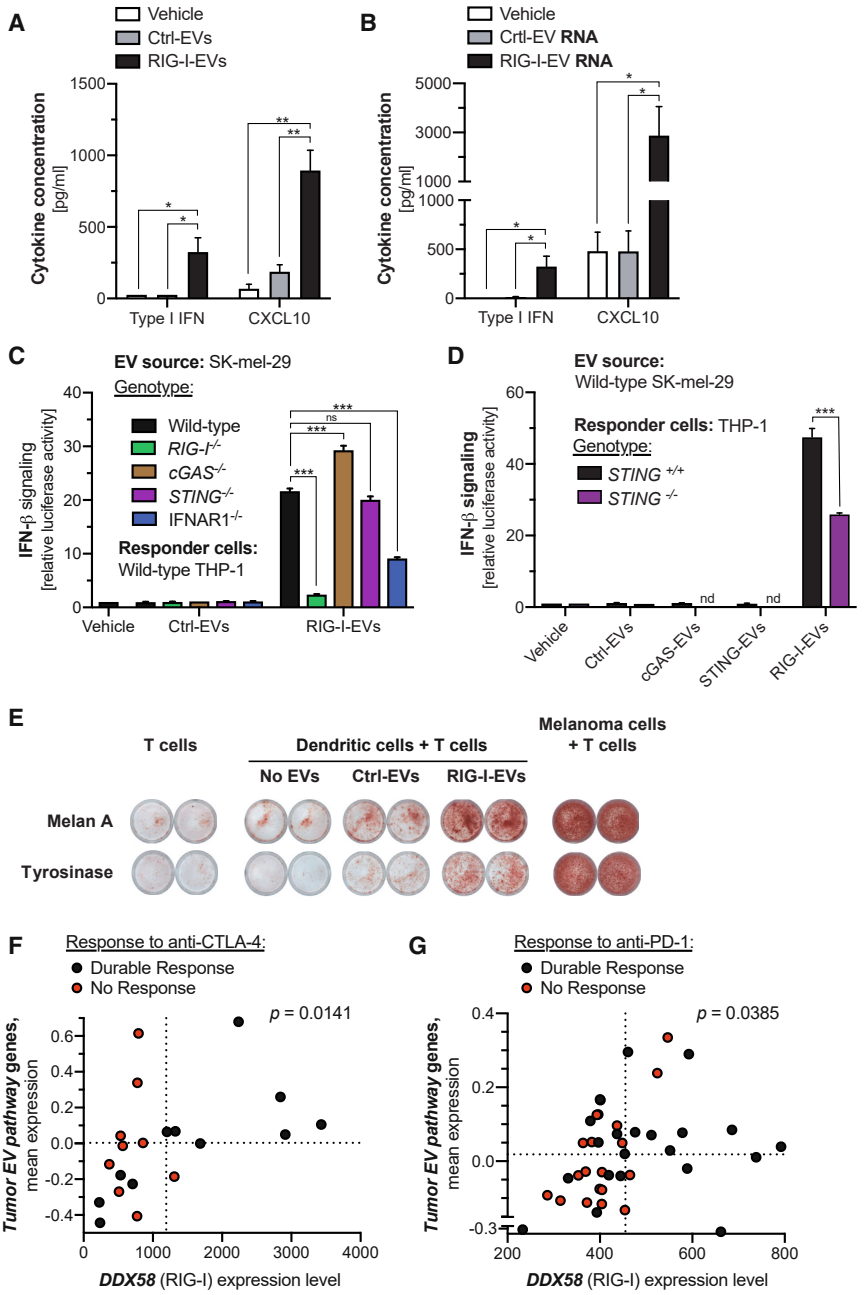

Figure 6. Tumor-intrinsic RIG-I activation in human melanoma mediates shuttling of immunostimulatory RNA within EVs and associates with beneficial clinical response

(A and B) Production of CXCL10 and IFN-I in human peripheral blood mononuclear cells (PBMCs) upon exposure to (A) human melanoma cell (D04mel)-derived RIG-I-EVs vs. Ctrl-EVs or (B) RNA purified from melanoma EV samples.

(C) IFN-I response in monocytic THP-1 reporter cells after exposure to EV samples derived from human melanoma cell lines with deficiency in RIG-I, cGAS, STING, or IFNAR1.

(D) IFN-I response in THP-1 cells with overexpression (*STING*$^{+/+}$) or gene-deficiency for *STING* (*STING*$^{-/-}$) upon exposure to different human melanoma EV preparations.

(E) Melanoma antigen-specific T cell response against Melan A (upper panel) or tyrosinase (lower panel) induced by melanoma EV samples in co-culture with autologous HLA-matched DCs (IFN-γ ELISpot, n = 2 technical replicates per group).

(F–G) Transcriptional activity of RIG-I-encoding *DDX58* and the *Tumor EV pathway* gene set in tumor samples from individual patients undergoing immune checkpoint inhibition. The dotted lines give mean transcriptional activity of the indicated genes. Gene expression and treatment response in (F) 20 melanoma patients treated with anti-CTLA-4 and (G) 41 melanoma patients treated with anti-PD-1.

All bar graphs show mean ± SEM of at least triplicate technical replicates, representative of at least two independent experiments. nd, not determined. See also Figures S7 and S8; Table S3.

We analyzed genome-wide transcriptional programs in 456 primary melanoma patient samples from The Cancer Genome Atlas (TCGA) determined by RNA-seq. Unfortunately, gene sets that are associated with specific EV release patterns are poorly defined. However, by screening 60 tumor cell lines, a recent study identified 25 commonly expressed genes whose expression level correlated with the total number of vesicles secreted specifically by tumor cells.[26] Indeed, we found for human melanoma samples in the TCGA that 24 genes of this predefined gene set were much more highly expressed in comparison to the remaining genome, and tended to be more transcriptionally active in tumor cells than in healthy tissue (Figures S8A and S8B). They were thus integrated as the *Tumor EV pathway* gene set for further analysis. In line with the current understanding of often pro-tumorigenic EV functions in the TME,[17] we found that high expression of the *Tumor EV pathway* gene set was associated with reduced overall survival in patients with malignant melanoma (Figure S8C). Patients with high *Tumor EV pathway* gene set expression were additionally stratified by median *DDX58* (the gene encoding for RIG-I) expression within the tumor samples. Within this unfavorable patient cohort with poor

(Figure 6D). However, IFN-I release induced by RIG-I-activated tumor EV samples was partly reduced in STING-deficient THP-1 cells (Figure 6D), suggesting that human tumor isEV preparations also contain immunostimulatory DNA. Similar to our findings in murine EVs, human melanoma EVs can shuttle TAAs such as Melan A, which was independent of RIG-I signaling in tumor cells (Figures S7G and S7H). Exposure of HLA-matched immature DCs to RIG-I-induced isEV samples from D05mel melanoma cells and subsequent co-culture with autologous T cell clones with receptor specificity for the melanoma antigens Melan A or tyrosinase resulted in cross-priming of tumor-antigen-specific T cells with potent IFN-γ release (Figure 6E).

overall survival, concomitantly high *DDX58* expression in melanoma samples was associated with a significantly prolonged survival (Figure S8D). In line with our previous findings on tumor-intrinsic *DDX58* transcript numbers,[12] multivariable Cox regression identified both high *Tumor EV pathway* gene set expression and low *DDX58* expression in melanoma samples as independent risk factors for death (Table S3A).

Based on the aforementioned challenges in the analysis of transcriptional programs in the context of EV biogenesis with no consensus on a universally defined "EV pathway" associated gene set, we validated this data analysis with a second, recently published, more broadly defined EV gene signature.[35] While the *Tumor EV pathway* signature adapted from Hurwitz et al.[26] only contains genes associated with EV production by tumor cells, the signature by Fathi et al.[35] represents multiple genes generally linked to EV production in a variety of different malignant and non-malignant cell types and is therefore hereafter referred to as the *Common EV pathway* gene set. The two signatures only overlap by two genes (*RAB7A* and *RALB*) and can thus be considered independent gene sets. The *Common EV pathway* gene set was not specifically active in human melanomas (Figures S8E and S8F). In line with our data in murine tumor samples (Figure 3A), we found that both EV pathway gene signatures' transcriptional activity in human melanoma samples strongly correlated with *DDX58* expression (Figure S8G), indicating a close relationship of EV biogenesis and activity of the RIG-I pathway. However, in contrast to the *Tumor EV pathway*, high expression levels of the *Common EV pathway* in human melanoma samples were not associated with reduced overall survival (Figure S8H). When analyzing the *Common EV pathway* and concomitant transcriptional activity of RIG-I-encoding *DDX58*, multivariable Cox regression did not identify high *Common EV pathway* gene set expression in melanoma samples as independent risk factor for death (Table S2B). These data suggest that transcriptional activity of genes modulating EV biogenesis seems to strongly differ between tumors and healthy tissue. In two independent cohorts of melanoma patients, simultaneously high transcriptional activity of both the *Tumor EV pathway* gene set and RIG-I-encoding *DDX58* was retrospectively associated with durable clinical response to ICB immunotherapy (Figures 6F and 6G). However, high *Tumor EV pathway* genetic activity was not an absolute predictive marker for treatment response, which is in line with the known existence of multiple other factors that co-drive treatment response.

DISCUSSION

The role of EVs in cancer progression is likely dynamic and specific to cancer type, genetics, and stage. Conditions under which cancer cells release immunostimulatory T cell-activating EVs remain unclear, but seem be dependent on external "triggers" such as genotoxic stress by chemotherapy or radiation therapy.[36,37] We here advance this concept and show that targeted activation of cancer-cell-intrinsic RIG-I signaling induces the generation of isEVs. These conditions of isEV release may be linked to each other, as genotoxic stress has been shown to result in intrinsic RIG-I activation by endogenous U1 and U2 RNA ligands in tumor cells.[33] In addition, tumor cell-intrinsic activation of the DNA receptor cGAS and, possibly, downstream signaling via STING have been implicated in tumor immunosurveillance and immunotherapy.[7,38] However, targeted activation of cGAS/STING in melanoma cells only induced poorly immunostimulatory EVs. This might be explained by the pathway's generally low activity in melanoma cells,[12] as the magnitude of effective cGAS/STING signaling in cancer cells has been shown to dictate effector responses.[39] As we found that release of isEVs in response to strong innate immune activation via RIG-I is a conserved cellular response pattern of various human and murine tumor cells types, cGAS/STING signaling may very well shape EV biogenesis and cargo in tumors with more active DNA sensing. To what extent such innate immune-regulated tumor EV release contributes to immunosurveillance during spontaneous tumor development (in the absence of strong external stimuli) remains to be determined.

At this time, it is unclear whether packaging of nucleic acids into EVs in response to active RIG-I signaling is a directed process or a mere stochastic event dependent on the abundance of certain nucleic acid sequences in the cytosol and/or endosome of tumor cells. Translocation of endogenous RIG-I ligands from the nucleus to the cytosol, as described for tumor cell stress situations,[33] may account for their preferred packing into RIG-I-EVs, as high abundance and cytoplasmic (vs. nuclear) location favor EV incorporation of specific RNAs.[32] The finding that active RIG-I signaling in tumor cells favors the shuttling of immunostimulatory RNAs within tumor EVs that subsequently engage the same pathway in recipient (immune) cells may suggest that the RIG-I protein or alternative RNA-binding proteins are actively involved in transporting RNA motifs to the intracellular vesiculation machinery.[32] Indeed, we did find RIG-I protein within murine B16 cell-derived EVs, but its abundance was independent of its activation status in EV-releasing tumor cells, arguing against a decisive RNA transporting function in regard to EV immunostimulatory capacity. Furthermore, we found different immunostimulatory RNA types within RIG-I-activated tumor-derived EVs that likely do not bind to RIG-I. The importance of the downstream transcription factors IRF3/7 further implicate an important role of active RIG-I and autocrine/paracrine IFN-I signaling for the generation of isEVs. Several components of the RIG-I pathway, including the receptor itself, are IFN-stimulated genes. Feedback loops via the IFN-I receptor have been shown to prime tumor cells for RIG-I-mediated effects.[40] Together, our data suggest that the RIG-I-IFN-I pathway in cancer cells regulates biogenesis and content packaging of exosomal EVs, which are subsequently released in a Rab27a-dependent manner.

Ctrl-EVs enriched from steady-state tumor cells had some antitumor activity but failed to induce long-term tumor control. This might suggest initiation of innate but not adaptive antitumor immune responses, independent of the IFN-I/DC/T cell axis. The involvement of NK cells in RIG-I-induced EV-mediated antitumor immunity falls in line with our recent study demonstrating that activation of RIG-I in melanoma cells results in the release of EVs with an increased expression of the NKp30 ligand on their surface, thus triggering NK-cell-mediated lysis of melanoma cells.[41] For RIG-I-induced isEVs, we observed potent antitumor synergism with anti-CTLA4/-PD1. We have previously shown that immunotherapy with ICB relies on both tumor and host immune cell-intrinsic RIG-I signaling.[12] Our current findings

suggest that RIG-I-induced EVs may shuttle immunostimulatory tumor-derived endogenous and exogenous RNAs to be detected in host immune cells to boost ICB efficacy. Accordingly, we found that high transcriptional activity of both RIG-I-encoding *DDX58* and a gene pattern associated with EV biogenesis in tumor samples were associated with improved overall survival of melanoma patients and beneficial clinical response to ICB with either anti-CTLA-4 or anti-PD-1. For this analysis, we used a predefined gene set whose gene products were identified to be associated with high EV production by screening 60 tumor cell lines.[26] However, our approach remains restricted by current limitations in the general understanding of EV biogenesis and its regulation. Intersections of the EV biogenesis pathway with other molecular pathways associated with the trafficking of intracellular vesicles (e.g., endocytosis) will inherently confound the interpretation of our gene expression studies, which will need to be verified by alternative methods. Furthermore, the ligands that activate RIG-I within tumor cells remain unclear and may comprise endogenous tumor RNA leaked into the cytosol under stress conditions, endogenous retroviral elements, or foreign bacterial RNAs. Also, under which conditions these RNAs are present in the cytosol and can activate RIG-I within tumor cells (for downstream isEV biogenesis) remains to be determined.

Our data also highlight the context-dependent, contrasting roles of EVs in the TME regarding immune activation and evasion. Numerous previous reports highlighted adversary effects of tumor EVs, which can inhibit immune cell function. In our study, generation of immunostimulatory EVs from various cancers strictly required previous RIG-I stimulation. Interestingly, tumor EVs enriched during steady-state conditions of untreated cancer cells did not actively promote tumor growth in our study. For future translational application of isEVs it will be essential to understand to which degree RIG-I signaling in tumor cells actively suppresses these immune-inhibitory functions of EVs or whether they are counterbalanced by strong immunostimulatory signals. Furthermore, endogenous ncRNAs in EVs also have the potential to activate cell-intrinsic pattern recognition receptors with detrimental outcome and progressive tumor growth. EV-mediated transfer of ncRNAs such as unshielded RN7SL1 RNA from stromal to breast cancer cells can activate both the RIG-I and NOTCH3 pathways, resulting in tumor growth and therapy resistance.[24,42] These data suggest that despite activation of the same pathway, the cellular source of EVs and also the conditions under which these EVs are generated can contribute to either immune evasion or antitumor efficacy. Nonetheless, using bulk tumor cell cultures isolated from freshly isolated melanoma tumor tissue, we confirm that production of RIG-I-induced isEVs is robust and not principally impaired by the inclusion of stromal cells in the TME known to potentially release inhibitory EVs.[26].

In sum, our findings uncover a hitherto unknown function of cytosolic nucleic acid sensors in cancer cells for the production and immunoregulatory function of tumor-derived EVs in both mice and humans. We identify the tumor cell-intrinsic RIG-I signaling pathway as a crucial mechanism to alter the composition of endogenous RNA within EVs and, thus, the immunostimulatory capacity of these vesicles. Given the availability of clinical-grade RIG-I agonists which are currently undergoing early phase 1/2 clinical testing (NCT03065023, NCT03739138, NCT02828098, NCT03203005, NCT03291002), targeting the RIG-I pathway in tumor cells may be a promising approach to beneficially "reprogram" the functionality of tumor cell-derived EVs.

Limitations of the study

Several questions remain to be addressed before a possible translational move of such "defined" cancer EV therapeutics into the clinic can be considered. (1) A precise analysis of the molecular mechanisms in the TME that determine the secretion of immunostimulatory vs. immunoinhibitory EVs upon stimulation with defined RIG-I agonists is required. (2) More data on isEVs in human subjects is needed to strengthen the translational relevance of our findings (e.g., by using patient-derived tumor organoid-immune cell co-cultures and/or xenograft models). (3) We followed an exploratory approach to gather sufficient functional information of murine and human tumor EVs in various different scenarios. Therefore, both EV cellular source and target cells differed for cell culture as well as *in vivo* systems to test tumor cell EVs for cancer treatment. Thus, we had to carefully titrate the amount of EVs for each experimental setting, even though the differences between EV concentrations in similar experimental scenarios were minimal. As effects of EV interactions with recipient cells could be concentration- and time-dependent, isEV dosages should be standardized for prospective use in advanced preclinical model systems. (4) The general efforts on standardizing the isolation and purification methods of EVs in the overall field have not brought us to a point that can match the potential of EVs for clinical use. At first, current challenges of good manufacturing practice-compliant manufacturing of cancer EVs, including insufficient large-scale manufacturing technologies and low yield, will need to be solved.

STAR★METHODS

Detailed methods are provided in the online version of this paper and include the following:

- KEY RESOURCES TABLE
- RESOURCE AVAILABILITY
  - Lead contact
  - Materials availability
  - Data and code availability
- EXPERIMENTAL MODEL AND STUDY PARTICIPANT DETAILS
  - Mice
  - Cell lines
- METHOD DETAILS
  - Generation of Rab27a deficient murine melanoma cells
  - Generation of gene deficient SK-mel-29 human melanoma cells
  - Reagents
  - Preparation of EVs and nucleic acid extraction
  - Murine bone marrow-derived dendritic cell culture
  - Quantification of cytokines
  - Western blot
  - Flow cytometry
  - Immunization with EVs
  - Tumor challenge and treatment

- Sequencing of murine EV-RNA
- Human PBMC EV stimulation
- ELISpot
- RNA-seq analysis of human melanoma samples
- Nanoparticle tracking analysis (NTA)
- Transmission electron microscopy
- Protein quantification with BCA assay
- Quantifying gene expression by real-time PCR
- Bulk murine melanoma RNA-sequencing
- Imaging flow cytometry

● QUANTIFICATION AND STATISTICAL ANALYSIS

SUPPLEMENTAL INFORMATION

Supplemental information can be found online at https://doi.org/10.1016/j.xcrm.2023.101171.

ACKNOWLEDGMENTS

This study was supported by Deutsche Forschungsgemeinschaft – Projektnummer 360372040 – SFB 1335 (to H.P. and F.B.), Projektnummer 395357507 – SFB 1371 (to H.P.), Projektnummer 324392634 – TRR 221 (to H.P.) and BA 2851/6-1 (to F.B.), German Cancer Aid (70114547 to H.P.), BZKF (TLG/05/R and SG AML to H.P.), the Wilhelm Sander Foundation (2021.041.1 to S.H., 2021.040.1 to H.P.), the European Hematology Association (to H.P.), the Bavarian State Ministry for Science and Art (to H.P.), DKMS Foundation for Giving Life (to H.P.), a Young Investigator award (Melanoma Research Alliance to S.H.), and the Germany José Carreras Foundation (DJCLS 07 R/2020 to S.H.). H.P. is supported by the EMBO Young Investigator Program.

AUTHOR CONTRIBUTIONS

S.H., F.S., and H.P. designed the research, and analyzed and interpreted the results. F.S., S.D., L.J., and S.E. conducted murine EV cell-culture and animal experiments. D.B. performed RNA-seq. A.G. performed imaging flow cytometry. C.W., C.M.S., N.L., and T.E. analyzed human and murine melanoma RNA-seq datasets. J.D.-P., K.F., S.L., and M.P. conducted experiments with human EVs. S.H. and H.P. prepared the manuscript. E.T.O., S.G., C.W., T.H., R.R., I.C.-C., W.H., B.G., J.R., F.B., C.C., and G.H. gave methodological support and conceptual advice. S.H. and H.P. guided the study.

DECLARATION OF INTERESTS

S.H. has been a consultant for Bristol Myers-Squibb (BMS), Novartis, Merck, Abbvie, and Roche, has received research funding from BMS and Novartis, and is an employee of and holds equity interest in Roche/Genentech. A.G. is a consultant for and has equity interest in Evox Therapeutics Ltd. and is inventor on several patent applications related to extracellular vesicles. B.G. is a scientific advisory board member of Innovex Therapeutics SL, PL BioScience, and Mursla Ltd, consultant for FUJIFILM Wako Chemicals, and a founding director of Exosla Ltd. G.H. is inventor on a patent covering synthetic RIG-I ligand, and co-founder of Rigontec GmbH. H.P. is a consultant for Gilead, Abbvie, Pfizer, Novartis, Servier, and BMS, and has received research funding from BMS.

Received: August 31, 2022
Revised: May 4, 2023
Accepted: August 3, 2023
Published: August 31, 2023

REFERENCES

1. Deng, L., Liang, H., Xu, M., Yang, X., Burnette, B., Arina, A., Li, X.D., Mauceri, H., Beckett, M., Darga, T., et al. (2014). STING-Dependent Cytosolic DNA Sensing Promotes Radiation-Induced Type I Interferon-Dependent Antitumor Immunity in Immunogenic Tumors. Immunity *41*, 843–852. https://doi.org/10.1016/j.immuni.2014.10.019.
2. Fischer, J.C., Bscheider, M., Eisenkolb, G., Lin, C.C., Wintges, A., Otten, V., Lindemans, C.A., Heidegger, S., Rudelius, M., Monette, S., et al. (2017). RIG-I/MAVS and STING signaling promote gut integrity during irradiation- and immune-mediated tissue injury. Sci. Transl. Med. *9*, eaag2513. https://doi.org/10.1126/scitranslmed.aag2513.
3. Poeck, H., Besch, R., Maihoefer, C., Renn, M., Tormo, D., Morskaya, S.S., Kirschnek, S., Gaffal, E., Landsberg, J., Hellmuth, J., et al. (2008). 5'-Triphosphate-siRNA: turning gene silencing and Rig-I activation against melanoma. Nat. Med. *14*, 1256–1263. https://doi.org/10.1038/nm.1887.
4. Woo, S.R., Fuertes, M.B., Corrales, L., Spranger, S., Furdyna, M.J., Leung, M.Y.K., Duggan, R., Wang, Y., Barber, G.N., Fitzgerald, K.A., et al. (2014). STING-Dependent Cytosolic DNA Sensing Mediates Innate Immune Recognition of Immunogenic Tumors. Immunity *41*, 830–842. https://doi.org/10.1016/j.immuni.2014.10.017.
5. Ablasser, A., and Hur, S. (2020). Regulation of cGAS- and RLR-mediated immunity to nucleic acids. Nat. Immunol. *21*, 17–29. https://doi.org/10.1038/s41590-019-0556-1.
6. Bartok, E., and Hartmann, G. (2020). Immune Sensing Mechanisms that Discriminate Self from Altered Self and Foreign Nucleic Acids. Immunity *53*, 54–77. https://doi.org/10.1016/j.immuni.2020.06.014.
7. Marcus, A., Mao, A.J., Lensink-Vasan, M., Wang, L., Vance, R.E., and Raulet, D.H. (2018). Tumor-Derived cGAMP Triggers a STING-Mediated Interferon Response in Non-tumor Cells to Activate the NK Cell Response. Immunity *49*, 754–763.e4. https://doi.org/10.1016/j.immuni.2018.09.016.
8. Schadt, L., Sparano, C., Schweiger, N.A., Silina, K., Cecconi, V., Lucchiari, G., Yagita, H., Guggisberg, E., Saba, S., Nascakova, Z., et al. (2019). Cancer-Cell-Intrinsic cGAS Expression Mediates Tumor Immunogenicity. Cell Rep. *29*, 1236–1248.e7. https://doi.org/10.1016/j.celrep.2019.09.065.
9. Hartmann, G. (2017). Nucleic Acid Immunity. Adv. Immunol. *133*, 121–169. https://doi.org/10.1016/bs.ai.2016.11.001.
10. Hornung, V., Ellegast, J., Kim, S., Brzózka, K., Jung, A., Kato, H., Poeck, H., Akira, S., Conzelmann, K.K., Schlee, M., et al. (2006). 5'-Triphosphate RNA is the ligand for RIG-I. Science *314*, 994–997. https://doi.org/10.1126/science.1132505.
11. Corrales, L., Glickman, L.H., McWhirter, S.M., Kanne, D.B., Sivick, K.E., Katibah, G.E., Woo, S.R., Lemmens, E., Banda, T., Leong, J.J., et al. (2015). Direct Activation of STING in the Tumor Microenvironment Leads to Potent and Systemic Tumor Regression and Immunity. Cell Rep. *11*, 1018–1030. https://doi.org/10.1016/j.celrep.2015.04.031.
12. Heidegger, S., Wintges, A., Stritzke, F., Bek, S., Steiger, K., Koenig, P.A., Göttert, S., Engleitner, T., Öllinger, R., Nedelko, T., et al. (2019). RIG-I activation is critical for responsiveness to checkpoint blockade. Sci. Immunol. *4*, eaau8943. https://doi.org/10.1126/sciimmunol.aau8943.
13. Poeck, H., Wintges, A., Dahl, S., Bassermann, F., Haas, T., and Heidegger, S. (2021). Tumor cell-intrinsic RIG-I signaling governs synergistic effects of immunogenic cancer therapies and checkpoint inhibitors in mice. Eur. J. Immunol. *51*, 1531–1534. https://doi.org/10.1002/eji.202049158.
14. Möller, A., and Lobb, R.J. (2020). The evolving translational potential of small extracellular vesicles in cancer. Nat. Rev. Cancer *20*, 697–709. https://doi.org/10.1038/s41568-020-00299-w.
15. van den Boorn, J.G., Dassler, J., Coch, C., Schlee, M., and Hartmann, G. (2013). Exosomes as nucleic acid nanocarriers. Adv. Drug Deliv. Rev. *65*, 331–335. https://doi.org/10.1016/j.addr.2012.06.011.
16. Pitt, J.M., Kroemer, G., and Zitvogel, L. (2016). Extracellular vesicles: masters of intercellular communication and potential clinical interventions. J. Clin. Invest. *126*, 1139–1143. https://doi.org/10.1172/jci87316.
17. Kosaka, N., Yoshioka, Y., Fujita, Y., and Ochiya, T. (2016). Versatile roles of extracellular vesicles in cancer. J. Clin. Invest. *126*, 1163–1172. https://doi.org/10.1172/jci81130.

18. Andre, F., Schartz, N.E.C., Movassagh, M., Flament, C., Pautier, P., Morice, P., Pomel, C., Lhomme, C., Escudier, B., Le Chevalier, T., et al. (2002). Malignant effusions and immunogenic tumour-derived exosomes. Lancet *360*, 295–305. https://doi.org/10.1016/s0140-6736(02)09552-1.

19. Wolfers, J., Lozier, A., Raposo, G., Regnault, A., Théry, C., Masurier, C., Flament, C., Pouzieux, S., Faure, F., Tursz, T., et al. (2001). Tumor-derived exosomes are a source of shared tumor rejection antigens for CTL cross-priming. Nat. Med. *7*, 297–303. https://doi.org/10.1038/85438.

20. Théry, C., Witwer, K.W., Aikawa, E., Alcaraz, M.J., Anderson, J.D., Andriantsitohaina, R., Antoniou, A., Arab, T., Archer, F., Atkin-Smith, G.K., et al. (2018). Minimal information for studies of extracellular vesicles 2018 (MISEV2018): a position statement of the International Society for Extracellular Vesicles and update of the MISEV2014 guidelines. J. Extracell. Vesicles *7*, 1535750. https://doi.org/10.1080/20013078.2018.1535750.

21. Nakase, I., and Futaki, S. (2015). Combined treatment with a pH-sensitive fusogenic peptide and cationic lipids achieves enhanced cytosolic delivery of exosomes. Sci. Rep. *5*, 10112. https://doi.org/10.1038/srep10112.

22. Besch, R., Poeck, H., Hohenauer, T., Senft, D., Häcker, G., Berking, C., Hornung, V., Endres, S., Ruzicka, T., Rothenfusser, S., and Hartmann, G. (2009). Proapoptotic signaling induced by RIG-I and MDA-5 results in type I interferon-independent apoptosis in human melanoma cells. J. Clin. Invest. *119*, 2399–2411. https://doi.org/10.1172/jci37155.

23. Duewell, P., Steger, A., Lohr, H., Bourhis, H., Hoelz, H., Kirchleitner, S.V., Stieg, M.R., Grassmann, S., Kobold, S., Siveke, J.T., et al. (2014). RIG-I-like helicases induce immunogenic cell death of pancreatic cancer cells and sensitize tumors toward killing by CD8(+) T cells. Cell Death Differ. *21*, 1825–1837. https://doi.org/10.1038/cdd.2014.96.

24. Nabet, B.Y., Qiu, Y., Shabason, J.E., Wu, T.J., Yoon, T., Kim, B.C., Benci, J.L., DeMichele, A.M., Tchou, J., Marcotrigiano, J., and Minn, A.J. (2017). Exosome RNA Unshielding Couples Stromal Activation to Pattern Recognition Receptor Signaling in Cancer. Cell *170*, 352–366.e13. https://doi.org/10.1016/j.cell.2017.06.031.

25. Poeck, H., Bscheider, M., Gross, O., Finger, K., Roth, S., Rebsamen, M., Hannesschläger, N., Schlee, M., Rothenfusser, S., Barchet, W., et al. (2010). Recognition of RNA virus by RIG-I results in activation of CARD9 and inflammasome signaling for interleukin 1 beta production. Nat. Immunol. *11*, 63–69. https://doi.org/10.1038/ni.1824.

26. Hurwitz, S.N., Rider, M.A., Bundy, J.L., Liu, X., Singh, R.K., and Meckes, D.G., Jr. (2016). Proteomic profiling of NCI-60 extracellular vesicles uncovers common protein cargo and cancer type-specific biomarkers. Oncotarget *7*, 86999–87015. https://doi.org/10.18632/oncotarget.13569.

27. Ostrowski, M., Carmo, N.B., Krumeich, S., Fanget, I., Raposo, G., Savina, A., Moita, C.F., Schauer, K., Hume, A.N., Freitas, R.P., et al. (2010). Rab27a and Rab27b control different steps of the exosome secretion pathway. Nat. Cell Biol. *12*, 19–30. https://doi.org/10.1038/ncb2000.

28. Mulcahy, L.A., Pink, R.C., and Carter, D.R.F. (2014). Routes and mechanisms of extracellular vesicle uptake. J. Extracell. Vesicles *3*, 24641. https://doi.org/10.3402/jev.v3.24641.

29. Desai, A.S., Hunter, M.R., and Kapustin, A.N. (2019). Using macropinocytosis for intracellular delivery of therapeutic nucleic acids to tumour cells. Philos. Trans. R. Soc. Lond. B Biol. Sci. *374*, 20180156. https://doi.org/10.1098/rstb.2018.0156.

30. Diamond, M.S., Kinder, M., Matsushita, H., Mashayekhi, M., Dunn, G.P., Archambault, J.M., Lee, H., Arthur, C.D., White, J.M., Kalinke, U., et al. (2011). Type I interferon is selectively required by dendritic cells for immune rejection of tumors. J. Exp. Med. *208*, 1989–2003. https://doi.org/10.1084/jem.20101158.

31. Fuertes, M.B., Kacha, A.K., Kline, J., Woo, S.R., Kranz, D.M., Murphy, K.M., and Gajewski, T.F. (2011). Host type I IFN signals are required for antitumor CD8+ T cell responses through CD8{alpha}+ dendritic cells. J. Exp. Med. *208*, 2005–2016. https://doi.org/10.1084/jem.20101159.

32. O'Brien, K., Breyne, K., Ughetto, S., Laurent, L.C., and Breakefield, X.O. (2020). RNA delivery by extracellular vesicles in mammalian cells and its applications. Nat. Rev. Mol. Cell Biol. *21*, 585–606. https://doi.org/10.1038/s41580-020-0251-y.

33. Ranoa, D.R.E., Parekh, A.D., Pitroda, S.P., Huang, X., Darga, T., Wong, A.C., Huang, L., Andrade, J., Staley, J.P., Satoh, T., et al. (2016). Cancer therapies activate RIG-I-like receptor pathway through endogenous non-coding RNAs. Oncotarget *7*, 26496–26515. https://doi.org/10.18632/oncotarget.8420.

34. Tanne, A., Muniz, L.R., Puzio-Kuter, A., Leonova, K.I., Gudkov, A.V., Ting, D.T., Monasson, R., Cocco, S., Levine, A.J., Bhardwaj, N., and Greenbaum, B.D. (2015). Distinguishing the immunostimulatory properties of noncoding RNAs expressed in cancer cells. Proc. Natl. Acad. Sci. USA *112*, 15154–15159. https://doi.org/10.1073/pnas.1517584112.

35. Fathi, M., Joseph, R., Adolacion, J.R.T., Martinez-Paniagua, M., An, X., Gabrusiewicz, K., Mani, S.A., and Varadarajan, N. (2021). Single-Cell Cloning of Breast Cancer Cells Secreting Specific Subsets of Extracellular Vesicles. Cancers *13*, 4397. https://doi.org/10.3390/cancers13174397.

36. Diamond, J.M., Vanpouille-Box, C., Spada, S., Rudqvist, N.P., Chapman, J.R., Ueberheide, B.M., Pilones, K.A., Sarfraz, Y., Formenti, S.C., and Demaria, S. (2018). Exosomes Shuttle TREX1-Sensitive IFN-Stimulatory dsDNA from Irradiated Cancer Cells to DCs. Cancer Immunol. Res. *6*, 910–920. https://doi.org/10.1158/2326-6066.Cir-17-0581.

37. Kitai, Y., Kawasaki, T., Sueyoshi, T., Kobiyama, K., Ishii, K.J., Zou, J., Akira, S., Matsuda, T., and Kawai, T. (2017). DNA-Containing Exosomes Derived from Cancer Cells Treated with Topotecan Activate a STING-Dependent Pathway and Reinforce Antitumor Immunity. J. Immunol. *198*, 1649–1659. https://doi.org/10.4049/jimmunol.1601694.

38. Harding, S.M., Benci, J.L., Irianto, J., Discher, D.E., Minn, A.J., and Greenberg, R.A. (2017). Mitotic progression following DNA damage enables pattern recognition within micronuclei. Nature *548*, 466–470. https://doi.org/10.1038/nature23470.

39. Gulen, M.F., Koch, U., Haag, S.M., Schuler, F., Apetoh, L., Villunger, A., Radtke, F., and Ablasser, A. (2017). Signalling strength determines proapoptotic functions of STING. Nat. Commun. *8*, 427. https://doi.org/10.1038/s41467-017-00573-w.

40. Boehmer, D.F.R., Formisano, S., de Oliveira Mann, C.C., Mueller, S.A., Kluge, M., Metzger, P., Rohlfs, M., Hörth, C., Kocheise, L., Lichtenthaler, S.F., et al. (2021). OAS1/RNase L executes RIG-I ligand-dependent tumor cell apoptosis. Sci. Immunol. *6*, eabe2550. https://doi.org/10.1126/sciimmunol.abe2550.

41. Daßler-Plenker, J., Reiners, K.S., van den Boorn, J.G., Hansen, H.P., Putschli, B., Barnert, S., Schuberth-Wagner, C., Schubert, R., Tüting, T., Hallek, M., et al. (2016). RIG-I activation induces the release of extracellular vesicles with antitumor activity. OncoImmunology *5*, e1219827. https://doi.org/10.1080/2162402X.2016.1219827.

42. Boelens, M.C., Wu, T.J., Nabet, B.Y., Xu, B., Qiu, Y., Yoon, T., Azzam, D.J., Twyman-Saint Victor, C., Wiemann, B.Z., Ishwaran, H., et al. (2014). Exosome transfer from stromal to breast cancer cells regulates therapy resistance pathways. Cell *159*, 499–513. https://doi.org/10.1016/j.cell.2014.09.051.

43. Gao, J., Aksoy, B.A., Dogrusoz, U., Dresdner, G., Gross, B., Sumer, S.O., Sun, Y., Jacobsen, A., Sinha, R., Larsson, E., et al. (2013). Integrative analysis of complex cancer genomics and clinical profiles using the cBioPortal. Sci. Signal. *6*, pl1. https://doi.org/10.1126/scisignal.2004088.

44. Chiappinelli, K.B., Strissel, P.L., Desrichard, A., Li, H., Henke, C., Akman, B., Hein, A., Rote, N.S., Cope, L.M., Snyder, A., et al. (2015). Inhibiting DNA Methylation Causes an Interferon Response in Cancer via dsRNA Including Endogenous Retroviruses. Cell *162*, 974–986. https://doi.org/10.1016/j.cell.2015.07.011.

45. Gide, T.N., Quek, C., Menzies, A.M., Tasker, A.T., Shang, P., Holst, J., Madore, J., Lim, S.Y., Velickovic, R., Wongchenko, M., et al. (2019). Distinct Immune Cell Populations Define Response to Anti-PD-1 Monotherapy and Anti-PD-1/Anti-CTLA-4 Combined Therapy. Cancer Cell *35*, 238–255.e6. https://doi.org/10.1016/j.ccell.2019.01.003.

46. Sauer, J.D., Sotelo-Troha, K., von Moltke, J., Monroe, K.M., Rae, C.S., Brubaker, S.W., Hyodo, M., Hayakawa, Y., Woodward, J.J., Portnoy, D.A., and Vance, R.E. (2011). The N-ethyl-N-nitrosourea-induced Goldenticket mouse mutant reveals an essential function of Sting in the in vivo interferon response to Listeria monocytogenes and cyclic dinucleotides. Infect. Immun. *79*, 688–694. https://doi.org/10.1128/iai.00999-10.

47. Caton, M.L., Smith-Raska, M.R., and Reizis, B. (2007). Notch-RBP-J signaling controls the homeostasis of CD8- dendritic cells in the spleen. J. Exp. Med. *204*, 1653–1664. https://doi.org/10.1084/jem.20062648.

48. Clausen, B.E., Burkhardt, C., Reith, W., Renkawitz, R., and Förster, I. (1999). Conditional gene targeting in macrophages and granulocytes using LysMcre mice. Transgenic Res. *8*, 265–277.

49. Seth, R.B., Sun, L., Ea, C.K., and Chen, Z.J. (2005). Identification and characterization of MAVS, a mitochondrial antiviral signaling protein that activates NF-kappaB and IRF 3. Cell *122*, 669–682. https://doi.org/10.1016/j.cell.2005.08.012.

50. Alexopoulou, L., Holt, A.C., Medzhitov, R., and Flavell, R.A. (2001). Recognition of double-stranded RNA and activation of NF-kappaB by Toll-like receptor 3. Nature *413*, 732–738. https://doi.org/10.1038/35099560.

51. Adachi, O., Kawai, T., Takeda, K., Matsumoto, M., Tsutsui, H., Sakagami, M., Nakanishi, K., and Akira, S. (1998). Targeted Disruption of the MyD88 Gene Results in Loss of IL-1- and IL-18-Mediated Function. Immunity *9*, 143–150. https://doi.org/10.1016/S1074-7613(00)80596-8.

52. Stetson, D.B., and Medzhitov, R. (2006). Recognition of Cytosolic DNA Activates an IRF3-Dependent Innate Immune Response. Immunity *24*, 93–103. https://doi.org/10.1016/j.immuni.2005.12.003.

53. Harshil Patel, P.E. (2023). Alexander Peltzer, Olga Botvinnik, Gregor Sturm, Denis Moreno, Pranathi Vemuri, silviamorins, Maxime U Garcia, Lorena Pantano. nf-core/rnaseq: nf-core/rnaseq v3.11.2 - Resurrected Radium Rhino.

54. Felix Krueger, F.J., Ewels, P., Afyounian, E., Weinstein, M., Schuster-Boeckler, B., and Hulselmans, G. (2023). TrimGalore: v0.6.10. https://doi.org/10.5281/zenodo.7598955.

55. Dobin, A., Davis, C.A., Schlesinger, F., Drenkow, J., Zaleski, C., Jha, S., Batut, P., Chaisson, M., and Gingeras, T.R. (2013). STAR: ultrafast universal RNA-seq aligner. Bioinformatics *29*, 15–21. https://doi.org/10.1093/bioinformatics/bts635.

56. Patro, R., Duggal, G., Love, M.I., Irizarry, R.A., and Kingsford, C. (2017). Salmon provides fast and bias-aware quantification of transcript expression. Nat. Methods *14*, 417–419. https://doi.org/10.1038/nmeth.4197.

57. Love, M.I., Huber, W., and Anders, S. (2014). Moderated estimation of fold change and dispersion for RNA-seq data with DESeq2. Genome Biol. *15*, 550. https://doi.org/10.1186/s13059-014-0550-8.

58. Sergushichev, A.A. (2016). An algorithm for fast preranked gene set enrichment analysis using cumulative statistic calculation. Preprint at bioRxiv. https://doi.org/10.1001/060012.

59. Hita, A., Brocart, G., Fernandez, A., Rehmsmeier, M., Alemany, A., and Schvartzman, S. (2022). MGcount: a total RNA-seq quantification tool to address multi-mapping and multi-overlapping alignments ambiguity in non-coding transcripts. BMC Bioinf. *23*, 39. https://doi.org/10.1186/s12859-021-04544-3.

60. Smit, A., Hubley, R., and Green, P.. RepeatMasker Open-4.0. http://www.repeatmasker.org.

61. Simon, S.R., and Ershler, W.B. (1985). Hormonal influences on growth of B16 murine melanoma. J. Natl. Cancer Inst. *74*, 1085–1088.

62. Reithmair, M., Buschmann, D., Märte, M., Kirchner, B., Hagl, D., Kaufmann, I., Pfob, M., Chouker, A., Steinlein, O.K., Pfaffl, M.W., and Schelling, G. (2017). Cellular and extracellular miRNAs are blood-compartment-specific diagnostic targets in sepsis. J. Cell Mol. Med. *21*, 2403–2411. https://doi.org/10.1111/jcmm.13162.

63. The Molecular Signatures Database (MSigDB). https://www.gsea-msigdb.org/gsea/msigdb/index.jsp.

64. Britten, C.M., Meyer, R.G., Frankenberg, N., Huber, C., and Wölfel, T. (2004). The use of clonal mRNA as an antigenic format for the detection of antigen-specific T lymphocytes in IFN-gamma ELISPOT assays. J. Immunol. Methods *287*, 125–136. https://doi.org/10.1016/j.jim.2004.01.026.

65. cgdsr: R-Based API for Accessing the MSKCC Cancer Genomics Data Server (CGDS). https://github.com/cBioPortal/cgdsr.

66. Snyder, A., Makarov, V., Merghoub, T., Yuan, J., Zaretsky, J.M., Desrichard, A., Walsh, L.A., Postow, M.A., Wong, P., Ho, T.S., et al. (2014). Genetic Basis for Clinical Response to CTLA-4 Blockade in Melanoma. N. Engl. J. Med. *371*, 2189–2199. https://doi.org/10.1056/NEJMoa1406498.

67. Macosko, E.Z., Basu, A., Satija, R., Nemesh, J., Shekhar, K., Goldman, M., Tirosh, I., Bialas, A.R., Kamitaki, N., Martersteck, E.M., et al. (2015). Highly Parallel Genome-wide Expression Profiling of Individual Cells Using Nanoliter Droplets. Cell *161*, 1202–1214. https://doi.org/10.1016/j.cell.2015.05.002.

68. Zhu, A., Ibrahim, J.G., and Love, M.I. (2019). Heavy-tailed prior distributions for sequence count data: removing the noise and preserving large differences. Bioinformatics *35*, 2084–2092. https://doi.org/10.1093/bioinformatics/bty895.

69. Subramanian, A., Tamayo, P., Mootha, V.K., Mukherjee, S., Ebert, B.L., Gillette, M.A., Paulovich, A., Pomeroy, S.L., Golub, T.R., Lander, E.S., and Mesirov, J.P. (2005). Gene set enrichment analysis: A knowledge-based approach for interpreting genome-wide expression profiles. Proc. Natl. Acad. Sci. USA *102*, 15545–15550. https://doi.org/10.1073/pnas.0506580102.

70. Erdbrügger, U., Rudy, C.K., Etter, M.E., Dryden, K.A., Yeager, M., Klibanov, A.L., and Lannigan, J. (2014). Imaging flow cytometry elucidates limitations of microparticle analysis by conventional flow cytometry. Cytometry A. *85*, 756–770. https://doi.org/10.1002/cyto.a.22494.

71. Headland, S.E., Jones, H.R., D'Sa, A.S.V., Perretti, M., and Norling, L.V. (2014). Cutting-edge analysis of extracellular microparticles using ImageStream(X) imaging flow cytometry. Sci. Rep. *4*, 5237. https://doi.org/10.1038/srep05237.

72. Görgens, A., Bremer, M., Ferrer-Tur, R., Murke, F., Tertel, T., Horn, P.A., Thalmann, S., Welsh, J.A., Probst, C., Guerin, C., et al. (2019). Optimisation of imaging flow cytometry for the analysis of single extracellular vesicles by using fluorescence-tagged vesicles as biological reference material. J. Extracell. Vesicles *8*, 1587567. https://doi.org/10.1080/20013078.2019.1587567.

73. Tertel, T., Bremer, M., Maire, C., Lamszus, K., Peine, S., Jawad, R., Andaloussi, S.E.L., Giebel, B., Ricklefs, F.L., and Görgens, A. (2020). High-Resolution Imaging Flow Cytometry Reveals Impact of Incubation Temperature on Labeling of Extracellular Vesicles with Antibodies. Cytometry A. *97*, 602–609. https://doi.org/10.1002/cyto.a.24034.

74. Inglis, H.C., Danesh, A., Shah, A., Lacroix, J., Spinella, P.C., and Norris, P.J. (2015). Techniques to improve detection and analysis of extracellular vesicles using flow cytometry. Cytometry A. *87*, 1052–1063. https://doi.org/10.1002/cyto.a.22649.

75. György, B., Módos, K., Pállinger, E., Pálóczi, K., Pásztói, M., Misják, P., Deli, M.A., Sipos, A., Szalai, A., Voszka, I., et al. (2011). Detection and isolation of cell-derived microparticles are compromised by protein complexes resulting from shared biophysical parameters. Blood *117*, e39–e48. https://doi.org/10.1182/blood-2010-09-307595.

STAR★METHODS

KEY RESOURCES TABLE

REAGENT or RESOURCE	SOURCE	IDENTIFIER
Antibodies		
Rat monoclonal anti-mouse IFN-β (clone RMMB-1)	PBL Assay Science	Cat#22400-1; RRID: AB_387846
Anti-mouse Interferon-beta rabbit serum	PBL Assay Science	Cat#32400-1; RRID: AB_387872
Anti-rabbit IgG coupled with horseradish peroxidase	Abcam	Cat#ab6721, RRID: AB_955447
Anti-human IFN-γ antibody (clone 1-D1K)	Mabtech	Cat#3420-3-250
Anti-mouse IFNaR1 antibody (clone MAR1-5A3)	BioXCell	Cat#BE0241; RRID: AB_2687723
Anti-mouse CTLA-4 antibody (clone 9H10)	BioXCell	Cat#BE0131; RRID: AB_10950184
Anti-mouse PD-1 antibody (clone RMP1-14)	BioXCell	Cat#BE0146; RRID: AB_10949053
Anti-mouse CD8a antibody (clone 2.43)	BioXCell	Cat#BE0118; RRID: AB_10949065
Anti-mouse CDNK1.1 antibody (PK136)	BioXCell	Cat#BE0036; RRID: AB_1107737
Western blot antibodies, see Table S5		
Flow cytometry antibodies, see Table S6		
Biological samples		
Human PBMCs from healthy donors	This paper	N/A
Chemicals, peptides, and recombinant proteins		
rmGM-CSF	Immunotools	Cat#12343123
rhGM-CSF	Peprotech	Cat#300-03
rhIL-4	Peprotech	Cat#200-04
Alt-R S.p. Cas9 Nuclease V3	IDT	Cat#1081058
DNAzol Reagent	Thermo Fisher	Cat#10503027
In vivo-jetPEI	PolyPlus	Cat#101000040
Lipofectamine 2000 Transfection Reagent	Thermo Fisher	Cat# 11668019
Critical commercial assays		
Total exosome isolation (from cell media) reagent	Thermo Fisher	Cat#4478359
Exo-spin mini	Cell Guidance Systems	Cat#EX01-25
Total Exosome RNA and Protein Isolation Kit	Thermo Fisher	Cat#4478545
Qubit 1X dsDNA HS Assay Kit	Thermo Fisher	Cat#Q33230
miRNeasy Mini Kit	Qiagen	Cat#217084
PKH67 Green Fluorescent Cell Linker Kit	Sigma-Aldrich	Cat#PKH67GL-1KT
Deep Red CellMask Plasma Membrane Stains	Invitrogen	Cat#C10046
SYTO RNASelect Green Fluorescent cell Stain	Invitrogen	Cat#S32703
iTAg MHC-I murine SIINFEKL tetramers	MBL	Cat#TS-5001-1C
Deposited data		
Murine B16 melanoma cell EV RNA-seq	This study	European Nucleotide Archive (ENA); PRJEB59517
RNA-seq human melanoma biopsies (TCGA databank)	Gao et al.[43]	cBioPortal skcm_tcga
RNA-seq healthy human skin tissue	GTEx Project	https://gtexportal.org; UBERON:0036149
Bulk tumor RNA-seq murine B16 melanoma	Heidegger et al.[12]	ENA; PRJEB32241
RNA-seq melanoma biopsies from anti-CTLA-4-treated patients	Chiappinelli et al.[44]	N/A
RNA-seq melanoma biopsies from anti-PD-1-treated patients	Gide et al.[45]	N/A

(*Continued on next page*)

Continued

REAGENT or RESOURCE	SOURCE	IDENTIFIER
Experimental models: Cell lines		
Murine: B16.OVA	Biocytogen	Cat#311537
Murine: B16 F10	ATCC	CRL-6475
Murine: CT26	ATCC	CRL-2638
Murine: 4T1	ATCC	CRL-2539
Murine: Panc02	CLS	Cat#300501; RRID: CVCL_D627
Human: THP1-Dual™ KI-hSTING-R232	InvivoGen	Cat#thpd-r232
Human: THP1-Dual™ KO-STING Cells	InvivoGen	Cat#thpd-kostg
Human: HEK-Blue IFN-α/β Cells	InvivoGen	Cat#hkb-ifnab
Human: SK-MEL-29	Laboratory of Barbara Schmidt	Cellosaurus CVCL_6031
Experimental models: Organisms/strains		
Mouse: C57BL/6J wildtype	Janvier Labs	C57BL/6JRj
Mouse: Sting$^{-/-}$ (Tmem173$^{gt/gt}$)	Sauer et al.[46]	N/A
Mouse: Itgax-Cre^{+}Ifnar1$^{f/f}$	Caton et al.[47]	N/A
Mouse: LysM-Cre^{+}Ifnar1$^{f/f}$	Clausen et al.[48]	N/A
Mouse: Mavs$^{-/-}$	Seth et al.[49]	N/A
Mouse: Tlr3$^{-/-}$	Alexopoulou et al.[50]	N/A
Mouse: Myd88$^{-/-}$	Adachi et al.[51]	N/A
Oligonucleotides		
3pRNA sequence: sense, 5′- UCA AAC AGU CCU CGC AUG CCU AUA GUG AGU CG -3′	Poeck et al.[3]	N/A
synRNA	Eurofins	N/A
Interferon-stimulating DNA (ISD)	Stetson et al.[52]	N/A
Primers for *mActin*, forward 5′-CACACCCGCCA CCAGTTCG-3′ backward 5′-CACCATCACACCCTGGTGC-3′	This paper	N/A
Primers for *mRab27a*, forward 5′-GCATTGATTTC AGGGAAAAGAGAG-3′ backward 5′-TTCTCCACACACCGCTCCATCCGC-3′	This paper	N/A
CRISPR sgRNA target sequences, see Table S4	This paper	N/A
Alt-R CRISPR-Cas9 tracrRNA	IDT	Cat#1072533
Recombinant DNA		
pSpCas9(BB)-2A-GFP (PX458)	Addgene	Addgene Plasmid #48138
Software and algorithms		
Flowjo	TreeStar	https://www.flowjo.com
nf-core/rnaseq v3.11.2	Patel et al.[53]	https://zenodo.org/record/3503887
Trim Galore!	Krueger et al.[54]	https://github.com/FelixKrueger/TrimGalore
STAR	Dobin et al.[55]	https://github.com/alexdobin/STAR/releases
Salmon	Patro et al.[56]	https://github.com/COMBINE-lab/Salmon
DESeq2	Love et al.[57]	https://bioconductor.org/packages/release/bioc/html/DESeq2.html
fgsea R package	Sergushichev et al.[58]	https://bioconductor.org/packages/release/bioc/html/fgsea.html
MSigDB	GSEA	https://www.gsea-msigdb.org/gsea/msigdb/index.jsp.
MGcount	Hita et al.[59]	https://github.com/hitaandrea/MGcount
RepeatMasker	Smit et al.[60]	http://www.repeatmasker.org.
cgdsr R package	CGDS	https://github.com/cBioPortal/cgdsr.
GraphPad Prism	Dotmatics	https://www.graphpad.com
R package cgdsr	CGDS	https://github.com/cBioPortal/cgdsr

RESOURCE AVAILABILITY

Lead contact

Further information and requests for resources and reagents should be directed to and will be fulfilled by the lead contact, Hendrik Poeck (hendrik.poeck@ukr.de).

Materials availability

The CRISPR-Cas9-edited murine and human melanoma cell lines generated for this study may be requested under a material transfer agreement as per institutional requirements from the lead contact.

Data and code availability

- RNA-sequencing of murine melanoma EV cargo data have been deposited to the European Nucleotide Archive (ENA) and are publicly available. The accession number is listed in the key resources table. This paper analyzes existing, publicly available data. The sources of these datasets are listed in the key resources table. Adjective data reported in this paper will be shared by the lead contact upon request.
- This paper does not report original code.
- Any additional information required to reanalyze the data reported in this paper is available from the lead contact upon request.

EXPERIMENTAL MODEL AND STUDY PARTICIPANT DETAILS

Mice

Female C57BL/6J mice were purchased from Janvier. Mice genetically deficient for *Mavs*, *Sting* (*Tmem173*$^{gt/gt}$), as well as Itgax-Cre^{+}Ifnar1$^{f/f}$ and LysM-Cre^{+}Ifnar1$^{f/f}$ transgenic mice have been described previously.[46–49] Mice were at least six weeks of age at the onset of experiments, had not been involved in previous procedures and were maintained in specific pathogen-free conditions. Wild-type and genetically deficient mice included in the same experiments were either littermates from heterozygous breeding or were co-housed for at least four weeks before the onset of experiments. Tumor growth of B16 melanoma has previously been reported to be similar in male and female mice.[61] Animal studies were approved by the local regulatory agency (Regierung von Oberbayern, Munich, Germany) and conformed to institutional and national guidelines and regulations. Mice genetically deficient for *Tlr3* or *Myd88* were only used as bone marrow donors and have been described previously.[50,51]

Cell lines

The B16 murine melanoma cell line expressing full-length chicken ovalbumin (here referred to as B16.OVA; male) was cultured in a complete DMEM medium supplemented with 400 μg/mL G418 (from Sigma-Aldrich). B16 F10 (male), CT26 (female), 4T1 (female), Panc02 (male) and NIH3T3 (male) cells were cultured in complete DMEM medium or RPMI medium, respectively. Human melanoma SK-MEL-5 (female), SK-MEL-29 (male), SK-MEL-30 (male), IGR-37 (male) and IGR-39 (male) cells were a gift from Barbara Schmidt (University of Regensburg) and were cultured in complete DMEM medium. Further, the human melanoma cell lines D04mel (sex unspecified), Ma-Mel-86b (female), or the ovarian cancer cell line Skov (female) were cultured in complete RPMI medium.

THP1-Dual KI-hSTING-R232 (Cat#thpd-r232, male) cells, THP1-Dual KO-STING (Cat#thpd-kostg, male) cells and HEK-Blue IFN-α/β (Cat#hkb-ifnab, female) Cells were purchased from InvivoGen (Toulouse, France). RPMI-1640 medium (Invitrogen) and DMEM (Invitrogen) were supplemented with 10% (v/v) FCS (EV-depleted by 100,000 G ultracentrifugation for 24 h at 4°C to minimize possible contamination with xenogenous EVs), 3 mM L-glutamine, 100 U/mL of penicillin and 100 μg/mL of streptomycin (all from Sigma-Aldrich). All cell lines were cultured in a humidified incubator with 5% CO_2 at 37°C.

METHOD DETAILS

Generation of Rab27a deficient murine melanoma cells

B16.OVA cells genetically deficient for Rab27a were engineered using the CRISPR-Cas9 system as described previously for clones deficient for RIG-I, IRF3/7, Caspase 3 or MLKL.[12] In brief, the Streptococcus pyogenes nuclease Cas9 in conjunction with various single guide (sg)RNAs was used to genetically edit B16.OVA cells. The specific target sequences of sgRNAs were designed for optimal on-target activity, and are listed in Table S4. The sgRNAs were cloned into pSpCas9(BB)-2A-GFP (pX458, a gift from Feng Zhang; Addgene plasmid #48138), which is a bicistronic expression vector containing Cas9 and a sgRNA. These constructs were transiently introduced into B16.OVA cells by lipofection using Lipofectamine 2000 in OptiMEM. After 6 h, the culture medium was removed and cells were provided with fresh medium. 24 h post transfection, GFP-expressing single-cell clones were isolated using fluorescence-activated cell sorting (FACS), and were expanded to monoclonal cell clines. Rab27a-deficiency was confirmed by immunoblotting and mRNA PCR.

Generation of gene deficient SK-mel-29 human melanoma cells

Gene-deficient SK-mel-29 cells (RIG-I, STING, cGAS, IFNAR1) were engineered using CRISPR-Cas9 technology. Two guide (g)RNAs (crRNAs, IDT, Leuven, Belgium) were designed to target each of the above genes, sequences are listed in Table S4 gRNAs were prepared using respective crRNA (200 μM) and Alt-R CRISPR-Cas9 tracrRNA (200 μM, IDT). The mixture was incubated for 5 min at 95°C in a ThermoCycler, and was cooled down to room temperature. Cas9 endonuclease protein (Thermo Fisher) was then mixed with two respective gRNAs to form ribonucleoprotein (RNP) complexes at room temperature for at least 20 min. Melanoma cells were prepared in P3 primary cell kit buffer (Lonza, Cologne, Germany). After mixing RNP complexes and cell suspensions in a PCR tube, the mixture was transferred to Nucleocuvette Strip (Lonza), and nucleofection was performed on the Lonza 4days nucleofector (Lonza) using program CM137. Then the cells were seeded in pre-warmed medium and cultured for 5–7 days. Bulk cells were collected for DNA isolation, gene knockout efficacy was determined by targeted PCR, TIDE sequencing, and/or immunoblotting.

Reagents

OptiMEM reduced serum medium was from Invitrogen. Double-stranded *in vitro*-transcribed 3pRNA (sense, 5′- UCA AAC AGU CCU CGC AUG CCU AUA GUG AGU CG -3′) was generated as described.[3] Synthetic dsRNA lacking the 5′-triphosphate (synRNA) was purchased from Eurofins (Ebersberg, Germany). A previously described 45-base pair non-CpG double-stranded DNA oligonucleotide (interferon stimulatory DNA, ISD)[52] was used for activation of cGAS/STING signaling in tumor cells. ISD single-strand oligonucleotides were purchased from Sigma-Aldrich (Munich, Germany) and were annealed by heating to 75°C for 30 min and re-cooling to room temperature (RT).

Preparation of EVs and nucleic acid extraction

Tumor cells were harvested, washed twice with PBS and were then seeded at a fixed concentration of $5x10^5$ cells per mL media containing 10% (v/v) EV-depleted FCS (to ~90% cell density). For *in vitro* transfection of tumor cells, nucleic acids were complexed with Lipofectamine 2000 (Life Technologies, Darmstadt, Germany) in OptiMEM (Invitrogen). Tumor cells were transfected with 3pRNA, synRNA (both 3 μg/mL) or ISD (6 μg/mL), or were left untreated. After 24 h, cell culture supernatants were collected, centrifuged at 400 G for 5 min, and subsequently 2,000 G for 30 min to remove cell debris and were then filtered through a Millex GV 220 nm PVDF membrane (Merck Millipore). Each sample of cell-free culture supernatant was transferred to a fresh tube. For precipitation-based EV purification, each sample was combined with ½ volume of 'Total Exosome Isolation Reagent (from cell media)' (Thermo Fischer) and mixed well by vortexing or pipetting up and down until a homogeneous solution was formed. Typical cell media volume utilized was 1 mL. The samples were incubated at 4°C overnight and then centrifuged at 4 °C at 10,000 G for 1 h. The supernatant was aspirated and discarded, and the EV pellet was resuspended in PBS buffer and stored at −80°C. EV pellets purified from 1 mL B16.OVA cell culture supernatant each were resuspended in 5 μL PBS (EV stock solution). Preparation of EVs by size-exclusion chromatography was performed with the "Exo-spin" kit (Cell GS, Cambridge, UK). Cell debris-depleted media was combined with ½ volume of "Exo-spin" precipitation buffer and mixed well, incubated overnight at 4°C and then centrifuged at 4°C and 16,000 G for 1h. The supernatant was discarded, and the EV-containing pellet was resuspended in PBS buffer before being applied to the size-exclusion chromatography column according to the manufacturer's instructions. Separation of EV subsets through differential ultracentrifugation was performed by sequential centrifugation of cell debris-depleted media with 2,000 G for 20 min, 10,000 G for 40 min, and 100,000 G for 90 min at 4°C. After each centrifugation step, the EV pellet was washed at the same speed for the same time before resuspension in 5 μL PBS buffer. EV-RNA was extracted with the 'Total Exosome RNA and Protein Isolation Kit' (Thermo Fisher) according to the manufacturer's instructions. RNA concentration was analyzed using the Qubit 1X dsDNA HS Assay Kit (Thermo Fisher) and RNA quality was assessed using the TapeStation System (Agilent). DNA was obtained using DNAzol reagent (Thermo Fisher) according to the manufacturer's protocol. In brief, 1 mL of DNAzol was added to isolated EVs. EVs were lyzed for 30 min at RT, and DNA was subsequently precipitated from the lysate with ethanol. Following an additional ethanol wash, DNA was solubilized in water. For some experiments, EVs were purified from 1:1 co-culture of B16.OVA melanoma cells and NIH3T3 fibroblasts, or from short-term cultures of bulk melanoma tumor tissue. To this end, subcutaneous melanoma tumors of approximately 1000 mm^3 were dissected, finely minced and filtered through a 100 μm nylon strainer (BD Bioscience), before single cell suspensions were cultured in DMEM supplemented with 10% EV-depleted FCS.

Murine bone marrow-derived dendritic cell culture

Murine bone marrow-derived DCs were generated by culturing bone marrow cells in complete RPMI medium supplemented with 20 ng/mL GM-CSF (Immunotools, Friesoythe, Germany). For EV stimulation, DC cultures were supplemented with 7 μL EV stock solution per 1 mL RPMI medium (corresponding to approximately 5×10^8 particles derived from 10^6 tumor cells per condition). In case of EVs derived from size exclusion chromatography, the stock solution applied to DCs was calibrated to include EVs from 1.4 mL tumor culture supernatant per 1mL RPMI. In some experiments, tumor EVs were mixed with Lipofectamine 2000 prior to BMDC exposure. As positive control, BMDCs were treated with *in vitro* transcribed 3pRNA (1 μg/mL) or ISD (2 μg/mL) using Lipofectamine 2000. As negative control, DCs were cultured under steady-state conditions ('Unstim.'), or with EVs enriched from tumor cell cultures exposed to just the transfection reagent lipofectamine (Vehicle-EVs). IFN-I secretion was determined by ELISA after 24 h. The expression of CD86 on BMDCs was quantified by flow cytometry after 24 h. To analyze uptake patterns, DCs were exposed to tumor EV samples that were labeled with the fluorescent membrane marker PKH67 (PKH67 Green Fluorescent Cell Linker Kit, Sigma-Aldrich). For some

experiments, the inhibitors dynasore (Sigma-Aldrich), amiloride (Sigma-Aldrich), D-Mannose (Fisher Scientific) and EDTA (Thermo Fisher) were added in the indicated concentrations. 10 μL of EV suspension were mixed with 50 μL of diluent and 0.4 μL PKH67 and incubated for 15 min at room temperature in the dark. Meanwhile Exosome Spin Columns (Invitrogen) were prepared according to the manufacturer's protocol. The labeled EVs were pipetted onto the Exosome Spin Columns and centrifuged at 750 G for 2 min. EV uptake in DCs was visualized by confocal fluorescent microscopy. 7 x 10^3 BMDCs were seeded in 18-well flat μ-slides (IBIDI) and incubated with PKH67 labeled EVs for 3 h at 37°C and 5% CO_2. Nuclei were stained with DAPI (2 μL/mL; Sigma-Aldrich) for 10 min and the cell membrane of DCs was stained with CellMask Deep Red plasma membrane stain (Invitrogen) according to the manufacturer's protocol. BMDCs were transfected with EV-extracted RNA (800 ng/mL) or DNA (140 ng/mL). For some conditions, RNA was treated with alkaline phosphatase (Apex, Epicentre) according to the manufacturer's protocol. In brief, 1 μL of Apex was added to EV-RNA (up to 1 μg) and incubated for 10 min at 37°C. The phosphatase was inactivated by heat inhibition for 5 min at 70°C. For RNA transfer experiments, EV RNA was labeled with SYTO RNASelect fluorescent cell stain (500 nM; Thermo Fisher) for 20 min at 37°C. Afterward, excessive stain was removed via Exosome Spin Columns (Invitrogen) which were prepared according to the manufacturer's protocol.

Quantification of cytokines

IFN-β concentration in murine cell culture supernatants was determined with a custom-made ELISA, as described previously.[12] In brief, Flat-bottom 96-well plates (Nunc) were coated with rat anti-mouse IFN-β antibody (PBL Assay Science Cat# 22400-1, RRID:AB_387846; 1 μg/mL) in coating buffer (eBioscience) for 16 h at 4°C. After extensive washing with PBS +0.5% Tween, the plate was blocked with PBS +10% FCS for 3 h on room temperature (RT). Samples were incubated on 4°C for 24 h, and plates were extensively washed. Anti-mouse Interferon-beta rabbit serum (PBL Assay Science Cat# 32400-1, RRID:AB_387872; 620 ng/mL) was added and incubated for 3 h at room temperature. After additional washing, polyclonal goat anti-rabbit IgG coupled with horseradish peroxidase (Abcam Cat# ab6721, RRID:AB_955447; 56 ng/mL) was added and incubated for 1 h at room temperature. After intensive washing, 100 μL of substrate solution (1xTBM Substrate, eBioscience) was added. When the reaction was complete, 100 μL of stop solution (2N H_2SO_4) was added to the substrate solution. Optical density of each well was immediately assessed, using a microplate reader set to 450 nm (Tecan). IFN-β production in human THP-1 monocytic cells was determined using the THP1-Dual KI-hSTING-R232 Cells reporter system (Invivogen). These cells are derived from the human THP1 monocyte cell line, which stably integrated a secreted inducible reporter construct to monitor type I IFN pathway activation. THP1 reporter cells were incubated for 24 h with EVs derived from control or 3pRNA-treated melanoma cells (40 μg/mL, determined via BCA assay), then type I IFN pathway activation was measured according to the manufacturer's instructions. PBMC culture supernatants were analyzed for cytokine secretion by ELISA (BD OptEIA Kits) or IFN-I release with the reporter cell line HEK-Blue IFN-α/β Cells (Invivogen) according to the manufacturers' protocol.

Western blot

Cells or EVs isolated from cell culture supernatants were solubilised in RIPA buffer (Pierce), separated by SDS-PAGE on 12% polyacrylamide gels and transferred onto a nitrocellulose blotting membrane (GE Healthcare). The membranes were blocked in 3–5% blocking reagent (GE Healthcare) in PBS-Tween (PBST) for 1 h at room temperature and incubated with respective antibodies (Abs) in 0.5–1% blocking reagent in PBST over night at 4°C. A list of antibodies used for Western blot can be found in Table S5. After 3 × 5 min washing in PBST, the peroxidase-conjugated secondary antibody was applied at 1:40,000 dilution in 1–2% blocking agent in PBST for 1.5 h at room temperature. After 3 × 5 min PBST washes, the bands were detected by Amersham ECL plus and developed on Amersham ECL developing film (GE Healthcare).

Flow cytometry

Cell suspensions were stained in PBS with 3% FCS. Fluorochrome-coupled antibodies were purchased from eBioscience or BioLegend and are listed in Table S6. For intracellular cytokine staining the Foxp3 Transcription Factor Fixation/Permeabilization Kit (eBioscience) was used. Data were acquired on a FACSCanto II (BD Biosciences) and analyzed using FlowJo software (TreeStar).

Immunization with EVs

For subcutaneous (sc) immunization, mice were injected sc in the hock of the hind leg with 6.25 μL EV stock solution (corresponding to approximately 8 x 10^9 particles per condition, based on preliminary titration experiments) derived from the indicated tumor cell cultures. The treatment was repeated at day 7. In some experiments, mice were pre-treated intraperitoneally (ip) with 400 μg anti-murine IFNaR1 antibody (clone MAR1-5A3, BioXCell, West Lebanon, NH) one day prior to the above immunization. On day 14, mice were sacrificed and draining lymph nodes and the spleen were removed. Lymphocytes of these organs were collected and *ex vivo* plated on a tissue-treated cell culture plate and cultured in the presence of 1 μg/mL OVA protein in complete RPMI medium for 72 h. IFN-γ levels of $CD8^+$ T cells were analyzed by flow cytometry and ELISA from culture supernatant.

Tumor challenge and treatment

For tumor challenge with therapeutic treatment, mice were injected subcutaneously (sc) with 10^5 B16.OVA cells or 2 x 10^6 Panc02 cells in the right flank on day 0. When tumors were readily visible, 18.75 μL EV stock solution derived from corresponding tumor cell

cultures (corresponding to approximately 2.4 x 10^{10} particles per condition, based on preliminary titration experiments) were injected in PBS peritumorally (pt). To exclude only localized innate immune responses, in some experiments mice were treated with subcutaneous (sc) isEV applications in tumor distant sites. Generally, injections were repeated 2 times (days 6, 9 and 12). In some experiments, anti-CTLA-4 (clone 9H10) and anti-PD-1 (clone RMP1-14) or appropriate isotype controls (200 μg, all from BioXCell, West Lebanon, NH) were additionally administered intraperitoneally (ip) at the same time points. Treatment with anti-CD8a (clone 2.43, BioXCell) or anti-NK1.1 (clone PK136) depleting antibodies was initiated two days prior to tumor induction (100 μg ip) and was repeated twice weekly (50 μg ip). For tumor rechallenge experiments, mice were injected iv with 10^5 B16.OVA melanoma cells. Naive mice were challenged with melanoma cells as controls. For *in situ* 3pRNA treatment, mice were injected sc with B16.OVA (2.4 x 10^5 right flank, 0.8 x 10^5 left flank) cells on day 0. Starting when tumors were readily visible (volume approximately 100 mm^3), 25 μg 3pRNA complexed in 3.5 μL in vivo-jetPEI (Polyplus) were repeatedly injected into the right-sided tumors on day 6, 9 and 12. Generally, mice were euthanized when the maximum tumor diameter exceeded 15 mm according to standard legal procedure (responsible state office Regierung von Oberbayern). Expansion of OVA-specific CD8 T cells was determined on day 15 after tumor induction using iTAg MHC-I murine SIINFEKL tetramers (Cat#TS-5001-1C, from MBL). At predefined time points, mice were sacrificed, and tumors as well as tumor-draining (inguinal) lymph nodes were removed using forceps and surgical scissors. Tumors and lymph nodes were minced and homogenized by filtering through a 100 μm nylon strainer (BD Bioscience). The cell suspensions were washed in PBS before subsequent analysis.

Sequencing of murine EV-RNA

RNA was extracted from EV samples using the miRNeasy Mini Kit (Qiagen) and eluted in 40 μL nuclease-free water. Prior to library preparation, RNAs were gently dried in a centrifugal evaporator, resuspended in 10 μL water and analyzed using capillary electrophoresis (RNA 6000 Pico Assay, 2100 Bioanalyzer, Agilent Technologies). Sequencing libraries were constructed from 6 μL of concentrated total RNA using the NEBNext Multiplex Small RNA Library Prep Set for Illumina (New England BioLabs) as previously.[62] PCR products were subjected to size selection by high-resolution gel electrophoresis and purity of libraries was assessed by capillary electrophoresis before running 50 cycles of single-end sequencing on the HiSeq2500 (Illumina). RNA-seq data was processed using the nf-core rnaseq pipeline.[53] In brief, sequencing reads were adaptor and quality trimmed using Trim Galore!,[54] and aligned to the GRCm38 reference genome using STAR.[55] Gene expression was quantified using Salmon,[56] and differential gene expression analyses were performed using DESeq2.[57] Gene set enrichment analysis was performed using the fgsea R package[58] and the Mouse MSigDB hallmark gene set.[63] To identify and quantify RNA biotypes in more detail, aligned sequencing reads were subjected to MGcount,[59] an RNA-seq quantification tool which hierarchically assigns reads to small RNA, long RNA exons, and long RNA introns accounting for length disparities and thus quantifies coding and non-coding transcripts. In addition, RepeatMasker[60] was run to identify and quantify interspersed repeats. If not stated otherwise, conservative thresholds for significantly regulated RNAs were set at a log2 fold change $\geq |1.5|$ and an adjusted p value of ≤ 0.05.

Human PBMC EV stimulation

Preparation of human PBMCs, human melanoma cell lines, human tumor EV generation, culture conditions, antibodies, reagents, and immunostimulatory oligonucleotides have been described before.[41] In brief, PBMCs were prepared by density gradient centrifugation using Biocoll (Sigma-Aldrich, #L6113) from peripheral blood of healthy donors. Human melanoma cells lines were cultured in RPMI with penicillin (1%) and streptomycin (1%) and 10% FCS (Gibco) in 10 cm dishes and at a confluence of 70–80% (5 × 10^6 cells), and were transfected with 3pRNA or poly-A RNA (ctrl RNA) as control. Therefore, 24 μg RNA were complexed with 60 μL Lipofectamine 2000 according to the manual and cells were incubated for 3 h with the transfection complexes. Afterward, cells were washed three times to remove lipofection complexes and cells were further cultured for 18 h in media supplemented with EV-reduced FCS for production of EVs. Supernatant of cells for EV purification was centrifugated for 5 min at 400 G and twice for 15 min at 10,000 G. Vesicles were pelleted twice at 100,000 G for 90 min with intermediate resuspension in PBS (SW32Ti Rotor, Beckman Coulter). The amount of EV protein (approximately 20–100 μg from 5 × 10^6 cells, dependent whether cells were activated with RIG-I ligand or not) was quantified by Bradford Assay (Carl Roth, #K015.2) or via Nanodrop (Peqlab, Erlangen, Germany). PBMCs were incubated with 10 μg/mL EVs with incubation times between 24 h and 48 h. IFN-I release was measured by HEK-Blue IFN-α/β reporter cells (Invivogen). To label particles released from human tumor cells, melanoma cells were incubated with 5 μM carboxyfluorescein succinimidyl ester (CFSE) (eBioscience, #65-0850-84). Subsequently, CFSE-positive particles were enriched from the melanoma culture supernatant as described above, and were exposed to PBMCs. Uptake of labeled particles by monocytes, NK cells, or T- and B cells was determined by flow cytometry. For generation of human immature DCs, Ficoll-separated PBMCs were used. In brief, PBMCs were adjusted to a density of 5x10^6/mL in RPMI medium and cells were plated for 1 h at 37°C. Later, non-adherent cells were removed and plastic-adherent cells were cultured for additional 24 h in RPMI supplemented with rhGM-CSF (1000 U/mL) and rhIL-4 (500 IU/mL), before EVs were added. 18 h later, the supernatant of DCs was analyzed for secretion of IFN-I using HEK-Blue IFN-α/β reporter cells.

ELISpot

IFN-γ ELISpot assays were performed as previously described.[64] Briefly, immature DCs were generated from HLA-A2 matched PBMC donors in the presence of IL-4 (500 IU/mL) and GM-CSF (1000 IU/mL) for 24 h, and were then exposed to EVs (75 μg/mL,

derived from D05mel human melanoma cells; EV dosage based on previously published experiments[41]) for additional 24 h. Melan A or tyrosinase sensitive autologous T cell clones were thawed and kept for 24 h in AIM-V medium supplemented with 10% human serum from healthy individuals and 250 IU/mL IL-2. ELISpot plates were coated with 10 μg/mL anti-human IFN-γ antibody (Mabtech, clone 1-D1K), and EV-loaded DCs (20,000 cells) were co-cultured with autologous T cells (10,000 cells) for 4 h. Control wells contained effector cells alone or effector cells in the presence of tumor cells (D05mel). Assay conditions were tested in triplicates. Assay development was done according to standard procedures using the biotinylated monoclonal antibody anti-hIFN-γ (Mabtech, 7-B6-1), and was analyzed using the KS ELISpot Automated Reader System. Spot numbers were determined with the use of a computer-assisted video image analysis program (KS ELISpot, Zeiss, Jena).

RNA-seq analysis of human melanoma samples

RNA-seq data and clinical data from the Cancer Genome Atlas (TCGA) were downloaded for 472 cutaneous melanoma samples from cBioPortal (study ID "skcm_tcga")[43] using the R package cgdsr.[65] Excluding patients with multiple tumors and missing or invalid overall survival data resulted in a cohort of 456 patients used for further analysis. *Tumor EV pathway* and *Common EV pathway* gene sets have been defined previously.[26,35] Of these, we excluded *Myosin Light Chain 3* (*MYL3*), since we found it not to be expressed in the 456 human melanoma samples, resulting in a *Tumor EV pathway* gene set of 24 genes. The melanoma patient cohorts under treatment with anti-CTLA-4[44,66] or anti-PD-1[45] for tumor RNA-seq analysis have been described previously. The gene expression level of each EV pathway gene was median centered and scaled by its median absolute deviation using its expression levels across all tumors within the cohort. Then, the mean of the centered and scaled EV pathway gene expression levels for one tumor sample was assigned as the mean EV pathway gene set expression value for that tumor sample. Using the median EV pathway gene set expression values of one cohort as a cut-off, tumor samples were assigned to a low or high EV pathway gene set expression subgroup for survival analysis. The significance of the association between concomitantly high transcriptional activity of *DDX58* and the *Tumor EV pathway* gene set with durable clinical response to either anti-CTLA-4 or anti-PD-1 (defined as complete response, partial response or stable disease for at least 6 months) was calculated with Fisher's exact test. Using an unbiased approach, median expression of the gene set was used as cutoff to classify patients into low and high expression subgroups. The data used for comparative RNA-seq analyses in healthy skin tissue were obtained from the Genotype-Tissue Expression (GTEx) Project.

Nanoparticle tracking analysis (NTA)

Sizing and quantification of EVs was performed with the NanoSight LM10 instrument, following the manufacturer's protocol, (NanoSight, Malvern Instruments Ltd, Malvern, UK). In brief, a 1 μL aliquot of obtained EV samples was diluted in $_{dd}H_2O$ (at least 1:1000) to achieve a uniform particle distribution, and 6 sequential measurements (1 min each) at 23°C (viscosity 0.09 cp) were performed. The instrument settings were: camera shutter 25–32 ms, 24.98–24.99 frames/s; drift velocity 5011 to 6970 nm/s; analysis: blur auto, detection threshold 5–6 multi, min track length auto and min expected size auto. At least 900 tracks were recorded per measurement.

Transmission electron microscopy

EV samples were diluted 1:50 in PBS. 5 μL of each diluted sample were applied to glow-discharged carbon grids, incubated for 60 s, blotted, briefly washed with $_{dd}H_2O$ and subsequently stained in 1% w/v uranyl acetate for 40 s. Images were recorded immediately using a CM200 at a nominal magnification of 50,000x on a Tietz4K camera. The pixel size on the specimen level was 0.21 nm.

Protein quantification with BCA assay

Protein load of EV samples was determined by bicinchoninic acid (BCA) assay using the Pierce BCA Protein Assay (Thermo Scientific) according the manufacturer's protocol. In brief, EVs were lyzed with RIPA buffer during an incubation time of 30 min on ice. After 1 min of vortexing, lysates were mixed with the kit reagents and incubated for 30 min on 37°C in the dark. The purple-colored reaction product of this assay exhibits a strong absorbance at 562 nm, which correlates linearly with protein concentrations. The absorbance was measured at or near 562 nm on a Tecan plate reader.

Quantifying gene expression by real-time PCR

Total RNA was isolated from cells lysed in TRIzol (Ambion) and was reversely transcribed using standard methods and kits according to manufactureŕs protocols (RNeasy Mini Kit, Qiagen; SuperScript III Reverse Transcriptase, Invitrogen). The specific primer pair sequences are listed below. Transcript amplification was visualized with the qPCR Core kit for SYBR Green I (Eurogentec) using a LightCycler 480 II (Roche) real-Time PCR system. The relative transcript level of each gene was calculated according to the $2-\Delta\Delta Ct$ method with normalization to β-Actin. The following mRNA primer sequences were used: *mActin* fwd 5′-CACACCCGCCAC CAGTTCG-3′, *mActin* rev 5′-CACCATCACACCCTGGTGC-3′, *mRab27a* fwd 5′-GCATTGATTTCAGGGAAAAGAGAG-3′, *mRab27a* rev 5′-TTCTCCACACACCGCTCCATCCGC-3′.

Bulk murine melanoma RNA-sequencing

RNA-seq library preparation, sequencing and archiving for this dataset have been published before.[12] The data are publicly available (European Nucleotide Archive, accession #: PRJEB32241). In brief, mice were injected subcutaneously with 2.4 x 10^5 B16.OVA

melanoma cells. On day 6, 25 μg 3pRNA complexed in 3.5 μL in vivo-jetPEI (Polyplus) were injected into the tumors. On day 7, tumors were removed and total cellular RNA was extracted from bulk tumor cells. Gencode gene annotations M24 and the mouse reference genome GRCm38 were derived from the Gencode homepage (EMBL-EBI). Drop-Seq tools v1.12[67] was used for mapping raw sequencing data to the reference genome. The resulting UMI filtered count matrix was imported into R v4.0.5 and lowly expressed genes were subsequently filtered out. Prior differential expression analysis with DESeq2,[57] dispersion of the data was estimated with a parametric fit using the group as response variable for the Generalized Linear Model (GLM). Apeglm[68] shrunken log2 foldchanges were calculated afterward, and used as input for the GSEAPreranked method.[69] Geneset definition was derived from a previous publication[26] Data was variance stabilized via the rlog function as implemented in DESeq2 and leading-edge genes from the GSEA-Preranked analysis were visualized as heatmap (z-transformed rlog expression values).

Imaging flow cytometry

In vitro transcribed 3pRNA was fluorescently labeled (FAM, excitation peak at 492 nm, emission peak at 518 nm) using the Silencer siRNA Labeling Kit (Thermo Fischer). B16.OVA cells were transfected with either unlabeled or FAM-labeled 3pRNA. After 48 h, EVs were isolated from cell culture supernatants as described above. Prior to analysis, 5 μL aliquots of EV stocks were thawed and diluted to a total volume of 50 μL by adding 45 μL of Dulbecco's PBS (Gibco Invitrogen) to each sample. Samples were then mixed and the total volume was acquired on an ImageStreamX MkII instrument (ISX; Amnis/MilliporeSigma) equipped with 5 lasers (70 mW 375 nm, 100 mW 488 nm, 200mW 561 nm, 150 mW 642 nm, 70 mW 785 nm, SSC). Only the 488 nm and 785 nm lasers were enabled at maximum powers, and data was acquired with 60x magnification, a 7 μm core size and low flow rate as described previously.[70,71] FAM signals were collected in channel 2 (480–560 nm filter), and channel 6 (745–800 nm filter) was used for SSC detection. Data analysis was performed using Amnis IDEAS software (version 6.1). The image display mapping was linearly adjusted on representative fluorescent particle/sEV images for each channel and then applied to all files of the respective experiment. Based on aforementioned previously described settings, optimized masking and gating settings were applied for data analysis.[72,73] For detergent lysis controls, samples were incubated for 30 min at RT after adding the non-ionic detergent Nonidet P-40 to a final concentration of 0.5% as described previously.[74,75]

QUANTIFICATION AND STATISTICAL ANALYSIS

If not stated otherwise, all data are presented as mean ± SEM. Statistical significance of single experimental findings was assessed with the independent two-tailed Student's *t* test. For multiple statistical comparisons of a dataset the one-way ANOVA test with Bonferroni or Dunnett's post-test was used. Overall survival was analyzed using the Log rank test. Significance was set at p values <0.05, $p < 0.01$, and $p < 0.001$ and was then indicated with an asterisk (*, ** and ***). If not stated otherwise, an asterisk without brackets indicates statistical comparison to 'Ctrl-EV'-treated cells. All statistical calculations were performed using Prism (GraphPad Software).